

PAPER • OPEN ACCESS

From the elastocaloric effect towards an efficient thermodynamic cycle

To cite this article: Parham Kabirifar *et al* 2022 *J. Phys. Energy* **4** 044009

View the [article online](#) for updates and enhancements.

You may also like

- [Elastocaloric effects of carbon fabric-reinforced shape memory polymer composites](#)
Seok Bin Hong, Yongsan An and Woong-Ryeol Yu
- [Elastic-like deformation and elastocaloric effect of a partly ordered iron-platinum alloy exhibiting a weak first-order martensitic transformation](#)
Takashi Fukuda and Tomoyuki Kakeshita
- [SMA foil-based elastocaloric cooling: from material behavior to device engineering](#)
F Bruederlin, H Ossmer, F Wendler et al.



PAPER

OPEN ACCESS

RECEIVED
19 July 2022REVISED
8 September 2022ACCEPTED FOR PUBLICATION
16 September 2022PUBLISHED
18 October 2022

Original content from
this work may be used
under the terms of the
[Creative Commons
Attribution 4.0 licence](#).

Any further distribution
of this work must
maintain attribution to
the author(s) and the title
of the work, journal
citation and DOI.



From the elastocaloric effect towards an efficient thermodynamic cycle

Parham Kabirifar , Jonas Trojer , Miha Brojan and Jaka Tušek*

Faculty of Mechanical Engineering, University of Ljubljana, Aškerčeva 6, 1000 Ljubljana, Slovenia

* Author to whom any correspondence should be addressed.

E-mail: Jaka.Tusek@fs.uni-lj.si**Keywords:** elastocaloric effect, shape memory alloys, thermodynamic cycle, phenomenological modelingSupplementary material for this article is available [online](#)

Abstract

In recent years, elastocaloric cooling technology has been considered as one of the most promising alternatives to vapor compression technology. Given that elastocaloric technology is only in the early stages of development, a uniform method for evaluating the elastocaloric effect has not yet been established, and the thermodynamics of different elastocaloric cooling cycles have not yet been studied in detail. Therefore, the main goal of this work is to investigate these two important areas. Here, multiple thermodynamic cycles were studied, focusing on the parameters of the holding period of the cycle, which is essential for heat transfer between the elastocaloric material and the heat sink/source. The cycles were applied to commercially available superelastic thin-walled NiTi tubes under compressive loading and a thin NiTi wire under tensile loading. Isostress cycles with constant stress throughout the holding period, isostrain cycles with constant strain throughout the holding period and no-hold cycles (without a holding period) were studied across multiple stress/strain ranges. Based on the experimental results, a previously developed phenomenological model was applied to better understand and further evaluate the different cycles. The results revealed that the applied thermodynamic cycle significantly affects the thermomechanical response and thus the cooling/heating efficiency of the elastocaloric material. We show that by using isostress cycles and partial transformations, a Carnot-like thermodynamic cycle with improved heating/cooling efficiency can be generated. By applying the isostress cycles, an adiabatic temperature change of 30.2 K was measured, which is among the largest directly measured reproducible adiabatic temperature changes reported for any caloric material to date. Ultimately, this study intends to serve as a basis for establishing a uniform method for evaluating the elastocaloric effect in different materials that would allow for reliable and accurate one-to-one comparison of the reported results in the rapidly growing field of elastocalorics.

1. Introduction

Alternative cooling/heat pumping technologies have recently attracted significant attention since current technologies, which are based mainly on vapor compression, are failing to comply with future demands on energy consumption and environmental protection. Apart from being over a century old, the great majority of vapor compression technologies suffer from relatively low efficiency, yet their main drawback throughout their development has been and still is the refrigerants that they use. The very first refrigerants used in vapor compression cooling were natural refrigerants, such as ether, ammonia, carbon dioxide and hydrocarbons. Nonetheless, their low efficiency, toxicity and flammability led to intensive research on alternative refrigerants [1, 2]. The breakthrough came with the synthesis of stable and efficient chlorofluorocarbons (CFCs). Later, however, the ozone-depleting effect of CFCs resulted in their ban and replacement by hydrofluorocarbons (HFCs). Once again, it turned out that HFCs should also be banned and replaced by other refrigerants because of their very high global warming potential. Along with the possible leakage of

refrigerants from cooling/heat pumping devices in the course of their installation, operation and maintenance, inappropriately disposing of such devices at the end of their life span would release considerable amounts of HFCs into the atmosphere [3, 4]. Since preventing the refrigerants from leaking into the atmosphere all around the globe is barely feasible, the next generation of refrigerants should be made from naturally occurring compounds [5]. Accordingly, we should either go back to where it all started, which is using natural refrigerants, such as carbon dioxide, ammonia and hydrocarbons, and try to overcome their inherent shortcomings or move towards alternative non-vapor compression cooling technologies by redefining the notion of refrigerant. Solid-state cooling/heat pumping technologies, such as electrocalorics, magnetocalorics, barocalorics and elastocalorics are some of the alternative cooling technologies [6–9], among which elastocalorics are recognized as the most promising non-vapor-compression cooling technology according to the U.S. Department of Energy and the EU Commission [10, 11].

In elastocaloric cooling/heat pumping, the latent heat of the martensitic phase transformation that is released/absorbed during loading/unloading of a superelastic material, such as a shape memory alloy (SMA) in its superelastic state, is utilized for heating/cooling [12]. The elastocaloric effect of different SMAs including NiTi-based [13–17], Cu-based [18, 19], Fe-based [20] and magnetic SMAs [21, 22], each of which have their pros and cons, can be found in the literature (see [12] for more information). Binary NiTi is the most studied SMA and is nowadays commercially available in different shapes, geometries and qualities. Of particular interest for elastocaloric applications, is thin-walled tubes, thin sheets and wires that allow for fast and efficient heat transfer due to their large surface-to-volume ratio. In addition to suitable geometry for efficient heat transfer, elastocaloric devices require durable operation with large elastocaloric effect without degradation upon cycling. Accordingly, elastocaloric effects in high-cycle regimes have been investigated in the literature [16, 23–25]. Prior to this work, the largest directly measured durable (after 1 000 000 fatigue cycles) adiabatic temperature change of 27 K was observed in thin-walled NiTi tubes under compression [26]. Although larger adiabatic temperature changes have been reported in the literature, for example, 58 and 40 K in a NiTi alloy at room temperature [27, 28], 38.5 K in a NiTi alloy at 120 °C [29] and 31.5 K in a Ni–Mn–Ti–B alloy [30], the reproducibility of these results was not investigated. As shown in [29], the adiabatic temperature changes decrease with training (thermomechanical stabilization) and get stabilized after about 100 cycles. Without training, the temperature changes and the mechanical response of the elastocaloric material are unstable and not reproducible, as is evident from the decrease in the adiabatic temperature changes from the first to the second cycle in [29] and the large residual strains after unloading in [27, 28].

Above the elastocaloric material level, several elastocaloric devices using different geometries and thermodynamic cycles have been designed and tested [31–42]. Although promising results in terms of temperature span and specific cooling/heating power have been achieved, the research on designing commercially viable elastocaloric devices that are durable and more efficient than their vapor compression counterparts is still ongoing. More comprehensive reviews of elastocaloric materials and devices can be found in the literature [12, 43].

1.1. The basics of the elastocaloric effect (martensitic transformation)

The phase transformation in NiTi is a non-diffusional (martensitic) phase transformation that, in its simplest form, occurs between an austenite phase, which has a high symmetry CsCl-type B2 cubic unit cell and a martensite phase, which has a low-symmetry B19' monoclinic phase (hereafter, these two specific crystalline structures are referred to as austenite and martensite). In general, depending on the temperature, upon application of an external stress field, an SMA can generate shape memory effects or superelasticity. Below the martensite finish temperature (M_f), shape memory effects can occur and above the austenite finish temperature (A_f), superelasticity, which is the basis of the elastocaloric effect, occurs. In both cases, the transformation is accompanied by a thermodynamic irreversibility [44, 45] that manifests itself as temperature and stress hysteresis (more details about the phase transformation can be found elsewhere [46]). In superelasticity, when the austenite is mechanically loaded, it transforms to the martensite (forward transformation) and the latent heat of the transformation is released [47]. Upon unloading, the opposite occurs (reverse transformation) and the latent heat is absorbed. The mechanical and thermal manifestations of the transformation are coupled. Consequently, superelasticity is stress/strain rate sensitive. To elaborate, two extremes can be considered. If the transformation occurs very slowly in infinitesimally small stress/strain steps, i.e. under isothermal conditions, the latent heat dissipates to the surroundings and the entropy of the material changes at a constant temperature. At the other extreme, i.e. under adiabatic conditions, the transformation occurs so rapidly that the sample cannot thermally interact with its surroundings. Thus, the released/absorbed latent heat and the consequent self-heating/cooling changes the temperature of the material itself (ΔT_{ad}). Due to thermomechanical coupling, self-heating/cooling suppresses the

transformation, meaning that, compared to isothermal conditions, higher/lower stresses are required to start/finish the forward/reverse transformation or to generate similar strains under adiabatic conditions.

The martensitic phase transformation and consequently the observed elastocaloric effect can be affected by numerous variables. Therefore, a one-to-one comparison of the existing results in the literature is difficult, if not impossible. The same elastocaloric material (i.e. the same geometry and chemical composition) can generate considerably different elastocaloric responses depending on its thermomechanical history and microstructure. For instance, modifying the grain size by severe plastic deformation and heat treatment [17], the presence or absence of precipitations [48] and texture [49] and even the size of the sample relative to the grain size and structure–microstructure interaction (size effects) [50–52] can significantly affect the phase transformation and consequently the elastocaloric response of the material. Moreover, testing conditions, such as the difference between the test temperature and A_f [53], loading mode (tension or compression) [12, 13], applied stress/strain, stress/strain rate [54], holding period parameters and training cycles can alter the observed elastocaloric effect [55]. The SMAs exhibit a tension-compression asymmetry [56], as a result of which the transformation mechanism and the response of SMAs under tensile loading and compressive loading are significantly different. In tension, the phase transformation occurs through discrete localized nucleation and growth events, while in compression, a uniform continuous transformation occurs. Therefore, in tension, the transformation plateau is almost flat but in compression, the transformation plateau is sloped (similar to strain hardening behavior). The transformation start/finish stresses, the maximum transformation strain and the hysteresis loop area are also different in tension and compression. As a consequence, the elastocaloric response of materials with identical chemical composition and microstructure would be completely different under tensile and compressive loading.

The efficiency of an elastocaloric material is usually expressed through the material's coefficient of performance (COP_{mat}) that is also used for material comparison. It is defined as the ratio between the cooling/heating energy and the input energy and can also be affected by the abovementioned variables. For instance, training significantly affects the hysteresis loop area, transformation stresses, transformation strain and the measured (adiabatic) temperature changes [26, 55, 57]. Moreover, an untrained sample has an unstable cyclic behavior and the response of the material, especially in the first few cycles of the training, can change drastically, implying that the elastocaloric response of the material is not reproducible either (in the untrained sample). In addition to the stable and reproducible responses, the elastocaloric material in a real elastocaloric device must undergo a certain thermodynamic cycle [58, 59]. The most widely applied thermodynamic cycle in elastocalorics is the Brayton cycle, which consists of four operational steps: adiabatic loading, holding period (heat transfer period), adiabatic unloading and holding period (heat transfer period). The holding period in the elastocaloric cycle allows for thermal interaction between the elastocaloric element and the heat transfer medium (or heat sink/source) and is crucial for generating useful cooling or heating power. Nonetheless, continuous cycling (without a holding period called no-hold cycles here) results in considerably high [16, 17] but not practically realistic COP_{mat} values, since useful cooling/heating power cannot be generated without the heat transfer that occurs during the holding period. Furthermore, in studies that have applied a holding period, the duration of the holding period and the parameter that has been held constant (typically strain rather than stress) have been chosen arbitrarily without considering the impact of these parameters on the elastocaloric effect. Above all, the applied stress/strain ($\Delta\sigma/\Delta\varepsilon$) and the magnitude of the transformation can significantly affect the adiabatic temperature changes (ΔT_{ad}), the specific heating/cooling energy (q_h/q_c), the input energy (w) and the COP_{mat} values.

1.2. Aims and goals

Since in the current state of the art, the parameters and conditions under which the elastocaloric effect has been measured and evaluated are mainly chosen arbitrarily, the aim of this work is to show, for the first time, the effects of the applied thermodynamic cycle (especially the holding period parameters) on the elastocaloric effect and its efficiency. Here, different elastocaloric thermodynamic cycles (no-hold, isostress and isostrain cycles), which were applied to NiTi tubes under compression and a NiTi wire in tension across different strain ranges, are comprehensively and systematically analyzed using both experimental (direct measurements) and theoretical (phenomenological modeling) approaches. Changing the parameters of the thermodynamic cycle alters its nature, and therefore drastically affects the achievable ΔT_{ad} and the accompanying $\Delta\sigma$ and $\Delta\varepsilon$, the specific heating/cooling energy, the input energy and the calculated COP_{mat} . It should be noted that, to date, the vast majority of elastocaloric cycles have been based on applying a constant strain during the holding period (isostrain conditions, e.g. [14, 18, 26, 60]) or have been applied without any holding period (no-hold cycles, e.g. [16, 17]). To the best of the authors' knowledge, the elastocaloric cycles under isostress conditions have not yet been evaluated (although quasi-isostress conditions were applied in some cases, e.g. [13, 61]). We show in this work that fixing the stress instead of the strain during the holding period allows for an additional transformation that leads to additional latent heat

release/absorption and more efficient thermodynamic cycles, which in some cases approach the Carnot thermodynamic cycle. Ultimately, this study intends to serve as a basis for establishing a uniform method for evaluating the elastocaloric effect in different materials that will allow a reliable and accurate one-to-one comparison of reported results in the rapidly growing field of elastocalorics. Although NiTi tubes and wires have been selected for this study, the findings are closely tied to the phase transformation mechanism and are generally applicable to any SMA of any geometry.

2. Materials and methods

2.1. Experimental

2.1.1. Materials and equipment

Experiments were performed on NiTi tubes under compression and a NiTi wire in tension. Two tubes with 18.18 mm gauge lengths, referred to as T1 and T2 hereafter, were cut using a low-speed diamond saw from a longer medical grade (compatible with ASTM F 2063) superelastic NiTi tube with an outer diameter of 3.70 mm and a wall thickness of 0.625 mm. The two ends of each tube were made flat, parallel to one another and perpendicular to the length of the tube by micromachining. According to the product datasheet (by Vasotube), the austenite finish temperature (A_f) of the tube with 55.95 wt.% Ni (approximately 50.88 at.% Ni) is between 0.7 °C and 1.5 °C. For tensile experiments, a wire of 1.5 mm diameter, 140 mm total length and 40 mm gauge length (referred to as W1 hereafter) with chemical composition and A_f (according to the product datasheet by SAES group) similar to those of the tubes was used. The reported A_f temperatures are in line with the observed room temperature superelasticity of T1, T2 and W1.

All mechanical tests were carried out under strain-rate controlled loading at room temperature (23 ± 1 °C) using a Zwick Z050 universal testing machine (UTM). For compression tests, a 50 kN Gassmann Theiss Messtechnik load cell with a maximum inaccuracy of $\pm 0.4\%$ across the entire measuring range of the load cell was used, and the displacement data were acquired using a long-stroke Zwick extensometer with an accuracy of ± 0.002 mm. To ensure the application of a uniaxial compressive force on the tubes, a custom-made holder [26] was used in all the experiments. It should be noted that because of the small size of the tubes, the extensometer is attached to the moving part of the holder rather than the tube itself (to have more accurate temperature measurements with an infrared camera). The extensometer was attached as close to the tube as possible to exclude the deformation of the UTM and most parts of the holder. However, the holder consists of multiple moving parts with different internal frictions. Therefore, the recorded mechanical response might be slightly different to the real response of the tube. For the tension tests, a 5 kN Xforce P-type Zwick/Roell load cell with a maximum inaccuracy of $\pm 1\%$ across the entire measuring range of the load cell was used, and for measuring the displacement (and subsequent strain calculations) the crosshead data were used. All stress and strain values are engineering values calculated based on the initial lengths and cross-sectional areas of the samples.

To capture the thermal response of the samples during the mechanical tests, they were first coated with a thin layer of black LabIR paint for standard applications with an emissivity of 0.92, and then the selected regions of interest were monitored with a FLIR A6750sc infrared camera at a frame rate of 120 Hz. The camera, which was equipped with a 50 mm focal length lens, has an absolute accuracy of $\pm 2\%$ of the temperature reading, a 640×512 pixel IR sensor with a spatial resolution of $15 \mu\text{m}$ and a noise-equivalent differential temperature of less than 20 mK. The measurement uncertainty of the temperature difference between the individual pixels, which determines the accuracy of capturing the temperature changes of the samples (the difference between a temperature peak and the ambient/initial temperature), is much smaller than the absolute temperature reading uncertainty of the camera. The regions of interest were squares with 2 mm long edges at the center of each tube and a 35 mm long line with 0.3 mm thickness in the middle of the wire. The reported temperature changes are the mean (averaged) values of the pixels within the regions of interest.

2.1.2. Training cycles

In order to achieve reproducible and stable thermal and mechanical responses, both tubes and the wire were first trained for 100 cycles (see table 1 for the details and appendix A, supplementary material for the results). At the beginning of the training cycles and all subsequent elastocaloric cycles, preloads (see table 1 for details) were applied to remove the displacements within the holder or the UTM parts. The recoverable strain of the last cycle of training for each sample (T1, T2 and W1), referred to as $\Delta\varepsilon_{\text{max}}$ hereafter, was considered as a reference to determine other strain ranges (fractions of $\Delta\varepsilon_{\text{max}}$) that were applied in the subsequent elastocaloric cycles (T1, T2 and W1 have $\Delta\varepsilon_{\text{max}}$ of 3.48%, 3.67% and 7.34%, respectively).

Table 1. The evaluated elastocaloric cycles and their parameters.

Sample	Pre-strain		Loading/unloading				
	Rate (s ⁻¹) ^a	Holding ^b	Rate (s ⁻¹) ^a	Range			Hold ^b
				Range	Max	Min	
Tube—Compression							
Preload	For all cycles, at 2.27×10^{-4} s ⁻¹ load to 170 MPa and unload to ~0.07% and hold the strain						
Training	N/A	N/A	2.27×10^{-3}	N/A	1140 MPa	10 MPa	N/A
Isostress	2.27×10^{-4}	Hold stress for 20 s	6.82×10^{-2} (Adiabatic)	$\Delta\varepsilon_1$ $\Delta\varepsilon_2$ $\Delta\varepsilon_3$ $\Delta\varepsilon_4$	$0.625 \times \Delta\varepsilon_{\max}^c$ $0.750 \times \Delta\varepsilon_{\max}$ $0.875 \times \Delta\varepsilon_{\max}$ $\Delta\varepsilon_{\max}$	$0.375 \times \Delta\varepsilon_{\max}$ $0.250 \times \Delta\varepsilon_{\max}$ $0.125 \times \Delta\varepsilon_{\max}$ 0.153%	Hold stress for 60 s
Isostrain S-comp		Hold strain for 20 s			Same as isostress ranges Two strain ranges: 1st range equal to isostrain/isostress ranges and 2nd range equal to ε at the end of holding periods of isostress ranges		Hold strain for 60 s
No-hold				$\Delta\varepsilon_1$ $\Delta\varepsilon_3$ $\Delta\varepsilon_4$	$0.625 \times \Delta\varepsilon_{\max}$ $0.875 \times \Delta\varepsilon_{\max}$ $\Delta\varepsilon_{\max}$	$0.375 \times \Delta\varepsilon_{\max}$ $0.125 \times \Delta\varepsilon_{\max}$ 0.153%	N/A
Isothermal	N/A	N/A	9.09×10^{-5}	N/A	$\Delta\varepsilon_{\max}$	0.005%	N/A
Wire—Tension							
Preload	For all cycles, at 2.27×10^{-4} s ⁻¹ load to 10 MPa and hold the stress						
Training	N/A	N/A	2.27×10^{-3}	N/A	565 MPa	10 MPa	N/A
Isostress	7.42×10^{-5}	Hold stress for 90 s	2.05×10^{-1} (Adiabatic)	$\Delta\varepsilon_1$ $\Delta\varepsilon_2$ $\Delta\varepsilon_3$ $\Delta\varepsilon_4$	$0.369 \times \Delta\varepsilon_{\max}$ $0.625 \times \Delta\varepsilon_{\max}$ $0.813 \times \Delta\varepsilon_{\max}$ $\Delta\varepsilon_{\max}$	1.72% 2.75% 2.22% 2.22%	Hold stress for 180 s
Isostrain S-comp		Hold strain for 45 s			Same as isostress ranges Two strain ranges: 1st range equal to isostrain/isostress ranges and 2nd range equal to ε at the end of holding periods of isostress ranges		Hold strain for 90 s
Isothermal	N/A	N/A	3.50×10^{-5}	N/A	$\Delta\varepsilon_{\max}$	10 MPa	N/A

^a In compression, identical for isostress, isostrain, s-comp and no-hold, and in tension, identical for isostress, isostrain and s-comp.

^b In compression, identical for isostrain, s-comp and no-hold, and in tension, identical for isostrain and s-comp.

^c T1, T2 and W1 have $\Delta\varepsilon_{\max}$ of 3.48%, 3.67% and 7.34%, respectively.

2.1.3. Elastocaloric cycles

The thermomechanical responses of the tubes (T1 and T2) and the wire (W1) were evaluated for three different elastocaloric cycles, namely isostrain cycles (constant strain throughout the holding period), isostress cycles (constant stress throughout the holding period) and no-hold cycles. In addition, strain compensation cycles (referred to as S-comp cycles hereafter) composed of a two-stage loading/unloading were applied to estimate the latent heat released/absorbed during the isostress holding period. However, the required strain rates (isothermal, adiabatic, training, etc) and holding period durations, which were determined experimentally, are different for the tubes under compression and the wire under tension

because of the tension-compression asymmetry of the phase transformation and the fact that different geometries and dimensions (tubes versus wires) have different heat transfer properties. Table 1 shows the parameters and description of the evaluated elastocaloric cycles.

Each cycle was evaluated at different strain ranges (later referred to as $\Delta\varepsilon_{ad}$) with respect to the $\Delta\varepsilon_{max}$. The evaluated strain ranges are equally distributed around the middle of the plateau (half of $\Delta\varepsilon_{max}$). In this way, the effects of applying partial transformation on the elastocaloric response of the samples that have different $\Delta\varepsilon_{max}$ could be investigated more accurately (see the note at the bottom of table 1). It should be noted that for the unloading, the minimum strain of $\Delta\varepsilon_4$ for the tubes and the minimum strains of all applied strain ranges for the wire were determined in such a way as to prevent exerting negative forces on the samples at the end of the adiabatic unloading (negative force is a consequence of the inevitable self-cooling and the UTM's limitation in decelerating appropriately near the end of the defined strain range). The self-cooling effect is more pronounced in tension, and the long thin wire is more prone to bending during the fast unloading. Therefore, the minimum strains are well above zero in tension. All of the cycles were applied around the middle of the transformation plateau of each tube and the wire, in order to avoid straining the so-called pure austenite and martensite phases, which do not contribute much to the generated adiabatic temperature changes but increase the magnitude of the applied stress/strain as discussed previously elsewhere [25]. Therefore, each cycle begins with a quasi-isothermal pre-straining to the maximum strain in each strain range. The pre-straining is followed by a short holding period with fixed stress for the isostress cycles and fixed strain for all other cycles to ensure thermally stabilized conditions. Subsequently, the samples are first adiabatically unloaded to the minimum strain in each strain range in all of the cycles.

The first adiabatic unloading is followed by a holding period during which the stress in the isostress cycles and the strain in the isostrain cycles and S-comp cycles are held constant for a given period of time so that the temperature of the sample equals the ambient temperature. After the first holding period of the isostress and the isostrain cycles, the samples are adiabatically loaded to the maximum strain of each cycle. The isostress and isostrain cycles were repeated three times across each strain range. Note that fatigue cycling is beyond the scope of this work. However, as previously shown in [25, 26], the elastocaloric effect does not degrade in a trained (stabilized) NiTi sample after several hundred thousand cycles. Accordingly, only three consecutive cycles were applied for each cycle and each strain range to check the repeatability of the thermomechanical response of the trained samples. In the no-hold cycles, which are only applied to T2 across three strain ranges, there are no holding periods, and the tube is continuously loaded/unloaded for 20 cycles. The S-comp cycles (applied to T2 and W1) are composed of two adiabatic loading and two adiabatic unloading segments per cycle, each of which is followed by a holding period with constant strain (see figure 5 for a visual description of the cycle). The strain limits of the first adiabatic loading/unloading segments of the S-comp cycles are equal to those of the isostress cycles of the same $\Delta\varepsilon$, while in the second adiabatic loading/unloading segments, the samples are loaded/unloaded to the strain that the corresponding isostress cycle reaches at the ends of its holding periods (note that there is an additional transformation during the holding period of the isostress cycles that generates the additional strain). The adiabatic temperature changes of the second adiabatic loading/unloading segment of the S-comp cycles are used to estimate the latent heat release/absorption during the additional non-adiabatic transformation that occurs during the holding period of the corresponding isostress cycles (because of experimental limitations, $\Delta\varepsilon_4$ was not applied to T2). To check the repeatability of the results, the S-comp cycles were repeated twice across each strain range. Finally, the isothermal cycles were applied to T2 and W1 across the complete transformation range ($\Delta\varepsilon_{max}$) and were used as input data for the phenomenological model.

2.2. Thermodynamic modelling

To support and better understand the experimental results, a thermodynamic model was used to evaluate the applied elastocaloric cycles. The model is based on a phenomenological model that was used to simulate the superelastic and shape memory response of SMAs and was originally presented in [62] and in more detail in [45]. The input data for the model, i.e. transformation strains, transformation temperatures, elastic moduli and Clausius–Clapeyron factors were obtained experimentally from isothermal response of the tubes under compression and the wire in tension. Figure 1 shows the stress–strain curves obtained experimentally and theoretically (using the phenomenological model). Figure 1 also shows the stress–strain response calculated by assuming a non-hysteretic behavior (averaging loading and unloading stress–strain curves). The model and the details of the fitting parameters are presented in appendix A, supplementary material.

Based on the modeled superelastic response of the material at different temperatures and by using basic thermodynamic relations (i.e. Maxwell relations), the elastocaloric response was calculated, and temperature–total entropy (T – s) diagrams were constructed, as shown in figure 2 (see appendix A, supplementary material for details). It is important to emphasize that entropy is a state function and consequently, the total entropy change is determined solely by the initial and final states of the material and is

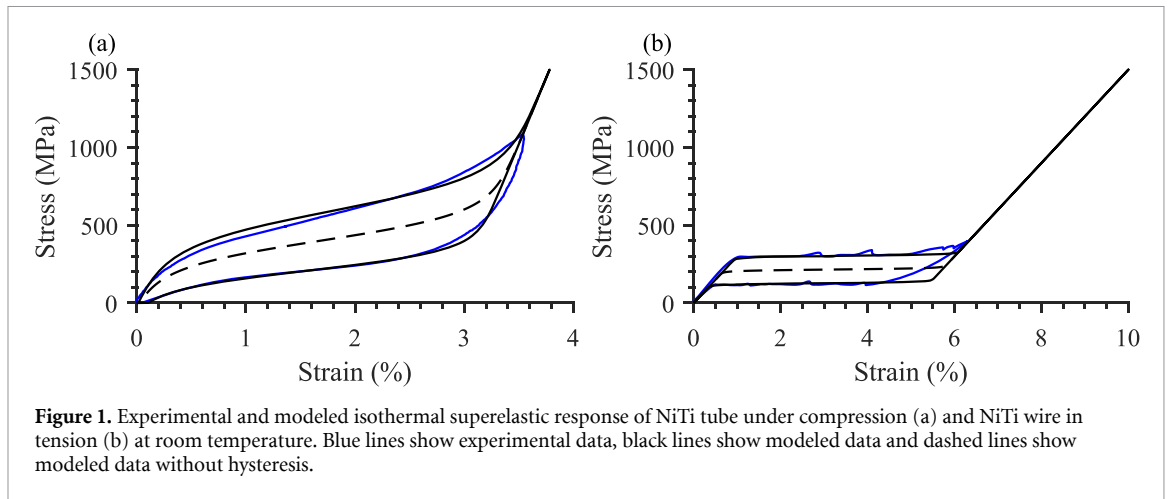


Figure 1. Experimental and modeled isothermal superelastic response of NiTi tube under compression (a) and NiTi wire in tension (b) at room temperature. Blue lines show experimental data, black lines show modeled data and dashed lines show modeled data without hysteresis.

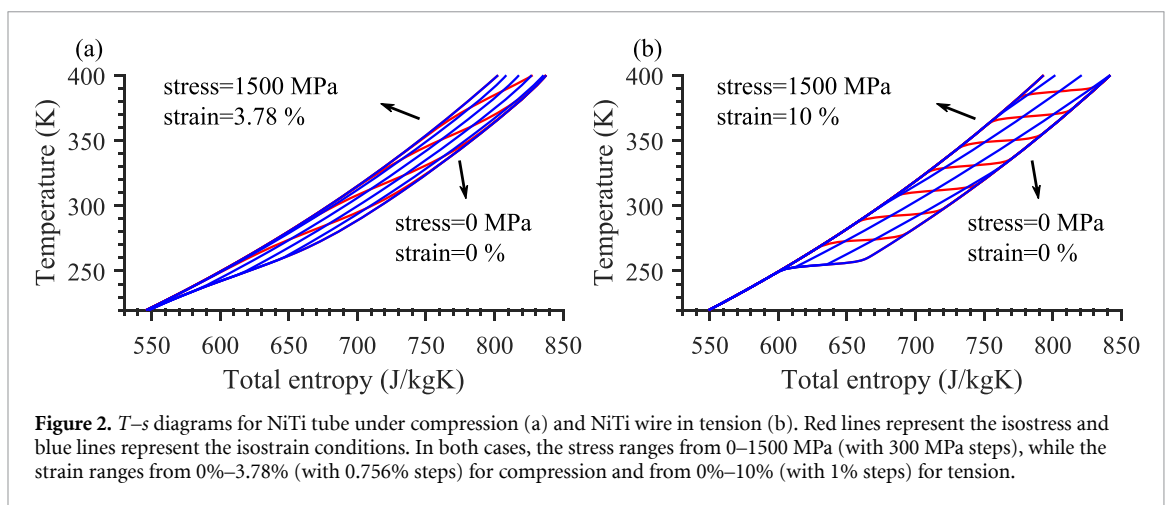


Figure 2. T - s diagrams for NiTi tube under compression (a) and NiTi wire in tension (b). Red lines represent the isostress and blue lines represent the isostrain conditions. In both cases, the stress ranges from 0–1500 MPa (with 300 MPa steps), while the strain ranges from 0%–3.78% (with 0.756% steps) for compression and from 0%–10% (with 1% steps) for tension.

independent of the path taken between the two states. Therefore, the T - s diagram is constructed using the non-hysteretic stress-strain behavior [45]. Since the aim of the theoretical analysis is to compare the isostress and isostrain cycles and understand their thermodynamic behavior, the hysteresis losses were not included in the model since doing so would have concealed the fundamental difference between the isostress and isostrain cycles.

Figure 2 shows T - s diagrams for compressive and tensile cycles. Different transformation mechanisms in tension and compression (tension-compression asymmetry) result in significantly different T - s diagrams. An almost entirely flat stress-strain transformation plateau in tension (figure 1(b)) leads to almost flat isostress lines between the total entropy values at zero and at the final stress/strain points, which is due to the fact that the entire entropy change at constant stress occurs across a very narrow temperature range (almost constant temperature). In compression, on the other hand, since the entropy change at constant stress occurs across a wider temperature range, the transformation plateau is steeper (figure 1(a)), resulting in steeper isostress lines. However, isostrain lines exhibit a significantly different trend due to a nonlinear mechanical behavior, i.e. the entropy change at constant strain occurs over much wider temperature ranges for both tension and compression, as discussed in [45]. The difference between the isostress and isostrain lines in the T - s diagram opens up new avenues for manipulating the elastocaloric cooling cycle by utilizing isostress or isostrain conditions.

3. Results and discussion

3.1. The importance of training

Training SMAs is crucial for achieving a reproducible and stable thermomechanical response. The reason is that, in practice, in a superelastic cycle, the martensitic phase transformation is neither completely reversible nor the only ongoing deformation process [63]. Consequently, during training under a fixed stress magnitude, the hysteresis loop area, total strain, recoverable strain, residual strain and temperature changes as well as the transformation start and finish stresses decrease in each consecutive cycle, while the

accumulated residual strain increases by cycling (see appendix A, supplementary material figure A.1). Towards the final cycles of the training, the residual strain becomes almost zero and the mechanical response of the material becomes repeatable and stable. The thermal response of the material tends to become stable somewhat earlier than its mechanical response [26].

On the one hand, the decrease in the recoverable strain and temperature changes upon training means that an untrained sample generates superficially higher ΔT_{ad} [26, 64]. On the other hand, the decrease in the transformation stresses and the hysteresis loop area means that the input work of an elastocaloric cycle is lower in a trained sample compared to an untrained sample. Therefore, assessing the elastocaloric performance of SMAs in an untrained state is not relevant to real applications because both the temperature changes and the input work, which are directly used to calculate the COP_{mat} , change significantly during training (see appendix A, supplementary material for details). Accordingly, directly comparing the elastocaloric response of a trained and an untrained material would be erroneous. In addition, an elastocaloric material can be used in a practical elastocaloric device only if it has a reproducible and durable thermomechanical response, which is not the case for untrained SMAs.

3.2. Thermomechanical response under different thermodynamic cycles

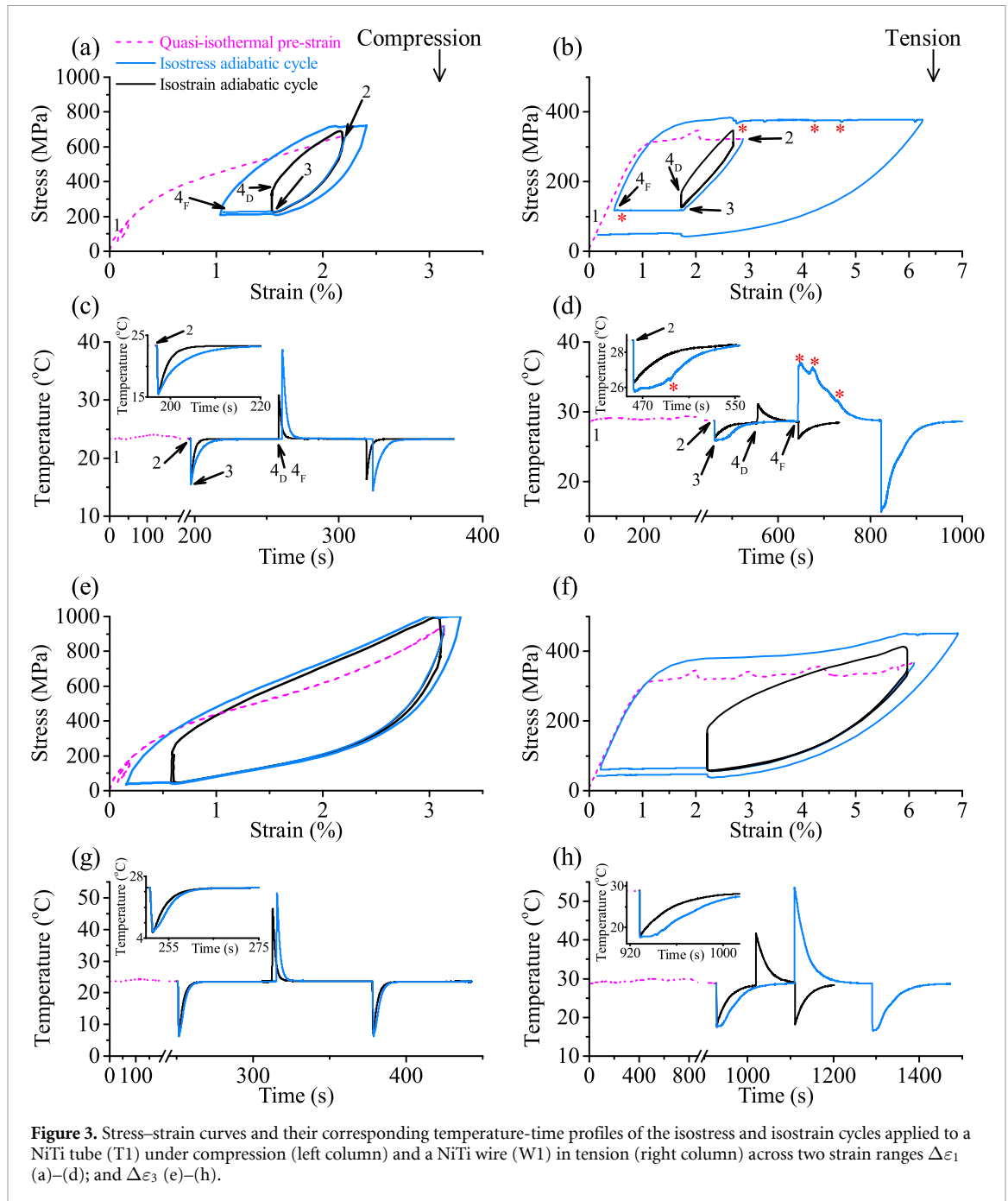
Figure 3 shows the representative stress–strain curves and the corresponding temperature–time profiles for the isostress and isostrain cycles applied to T1 and W1 under compression and tension across $\Delta\varepsilon_1$ and $\Delta\varepsilon_3$ (two of the four applied strain ranges). The results for the other two ranges ($\Delta\varepsilon_2$ and $\Delta\varepsilon_4$) are shown in appendix A and supplementary material figure A.2.

The martensitic transformation responsible for the elastocaloric effect has a thermomechanical coupling that results in a direct connection between the thermal and mechanical states of the samples and accordingly, the equilibrium state of the sample is determined by a combination of stress/strain and temperature. The applied stress/strain also indicates the magnitude of the transformation and the resulting phase fraction, which is the proportion of the austenite to the martensite present in the sample. In addition to the ambient temperature, accumulation of the released/absorbed transformation latent heat during a fast loading/unloading (self-heating/cooling) changes the temperature of the sample and thus shifts the stress/strain–temperature equilibrium or more precisely the phase fraction–temperature equilibrium. This also results in a rate-dependent mechanical response of the samples (different mechanical responses under isothermal and adiabatic conditions of identical $\Delta\varepsilon$).

In both tension and compression in figure 3, a small broad symmetrical peak with a minor temperature change is observed during the initial quasi-isothermal (very slow) loading (dashed magenta lines from point 1 to point 2 in figure 3), while the subsequent adiabatic peaks are sharp and asymmetrical. Due to the minor temperature changes and the absence of a pronounced self-heating during the initial quasi-isothermal loading, it can be safely assumed that in both the isostress and the isostrain cycles before the first adiabatic unloading (point 2), the samples have similar initial conditions with respect to their absolute temperature (equal to the ambient) and equilibrium phase fractions. Therefore, the first adiabatic unloading, from point 2 to point 3, ends at a similar stress/strain in both the isostress and the isostrain cycles and thus generates similar ΔT_{ad} , as shown in figures 3(c), (d), (g) and (h) and their insets.

The difference between the isostress and isostrain cycles begins at point 3 (figure 3), where the first holding period is applied to the samples and the temperature of the samples increases from the generated T_{ad} ($T_{ad} = T_{amb} - \Delta T_{ad, 1st\ unloading}$) towards the ambient air temperature (T_{amb}). This gradual temperature change demands a gradual transition from stress/strain– T_{ad} towards stress/strain– T_{amb} equilibrium. Therefore, the magnitude of the transformation and the corresponding phase fraction can change accordingly. Since the strain in the isostress cycles can freely change during the holding period, the additional transformation (austenite to martensite after adiabatic loading and the reverse after adiabatic unloading) can progress (from point 3 to point 4_F—see figure 3) and the new equilibrium is reached. This equilibrium is identical to that of an isothermal cycle under the same stress (as clearly observable in figure 3(b), where point 4_F coincides with the quasi-isothermal magenta line). In the isostrain cycles, on the other hand, where the strain is constrained during the holding period, this additional transformation does not occur because there is no room for the required change in the transformation strain. Therefore, the sample does not reach the required equilibrium phase fraction and only stress relaxation (point 3 to point 4_D—see figure 3) occurs with the temperature change [65].

As the additional transformation occurs over the holding period of the isostress cycles, additional latent heat is released/absorbed throughout this process. Therefore, as shown in figures 3(c) and (d) and their insets, the sample heats up (towards the ambient) during the holding period by convection to the air and conduction through the grips, but the additional transformation and latent heat absorption under the isostress holding conditions slows down the temperature increase compared to the isostrain cycles. Since the transformation and the latent heat release/absorption during compression is uniform, only the slope of the



temperature–time profile changes during the holding period under isostress conditions (see figure 3(c) and supplementary video B1 in appendix B). In tension, on the other hand, where nonuniform transformation occurs during the holding period, the nucleation and growth of the austenite phase are clearly seen as sharp peaks (some marked with red asterisks) on the stress–strain curves and the temperature–time profiles in figures 3(c) and (d). This is also clearly visible in the IR videos shown in supplementary video B2 in appendix B. As shown in figures 3(a), (b), (e) and (f), as a result of the additional transformation during the holding period of an isostress cycle, the strain at the end of the first holding period of the isostress cycle is significantly larger than that of the isostrain cycle especially in tension. Compared to the isostrain cycles, the samples that undergo an isostress cycle always reach the equilibrium phase fraction and consequently generate larger strain and larger transformation at the end of the holding period and therefore generate larger ΔT_{ad} when subsequently loaded adiabatically to fixed target strain, as shown in figures 3(c)–(f). Compared to compression, with its inherently sloped transformation plateau, the flat plateau in tension results in much larger additional phase transformation and therefore larger latent heat release/absorption and larger total entropy change during the holding period. In tension, this additional transformation occurs through multiple discrete nucleation and growth events (see appendix B, supplementary videos) and as a

consequence, since each nucleation and growth event decreases/increases the temperature significantly (see the inset of figure 3(d)), the wire requires a longer time to reach the ambient air temperature compared to the tube under compression, which undergoes a homogeneous transformation. Accordingly, in tension, the maximum temperature in figure 3(d) is generated non-adiabatically through a large nucleation during the holding time and immediately after the first adiabatic loading (a non-adiabatic maximum temperature change was mentioned in [13] but not investigated further).

As can be seen in figures 3(e)–(h), as the applied adiabatic strain range increases and gets closer to $\Delta\varepsilon_{\max}$ (more complete transformation during the adiabatic loading/unloading) there are less untransformed phases after the adiabatic loading/unloading; therefore, the magnitude of the additional transformation during the isostress holding periods decreases and the isostress and the isostrain cycles become more similar. Nevertheless, since the transformation-suppressing effect of the self-heating/cooling is always present during the adiabatic loading/unloading, the isostress and isostrain cycles would always have different outcomes, although less pronounced at larger $\Delta\varepsilon$.

3.3. Elastocaloric performance in different thermodynamic cycles—experimental results

3.3.1. Adiabatic temperature changes

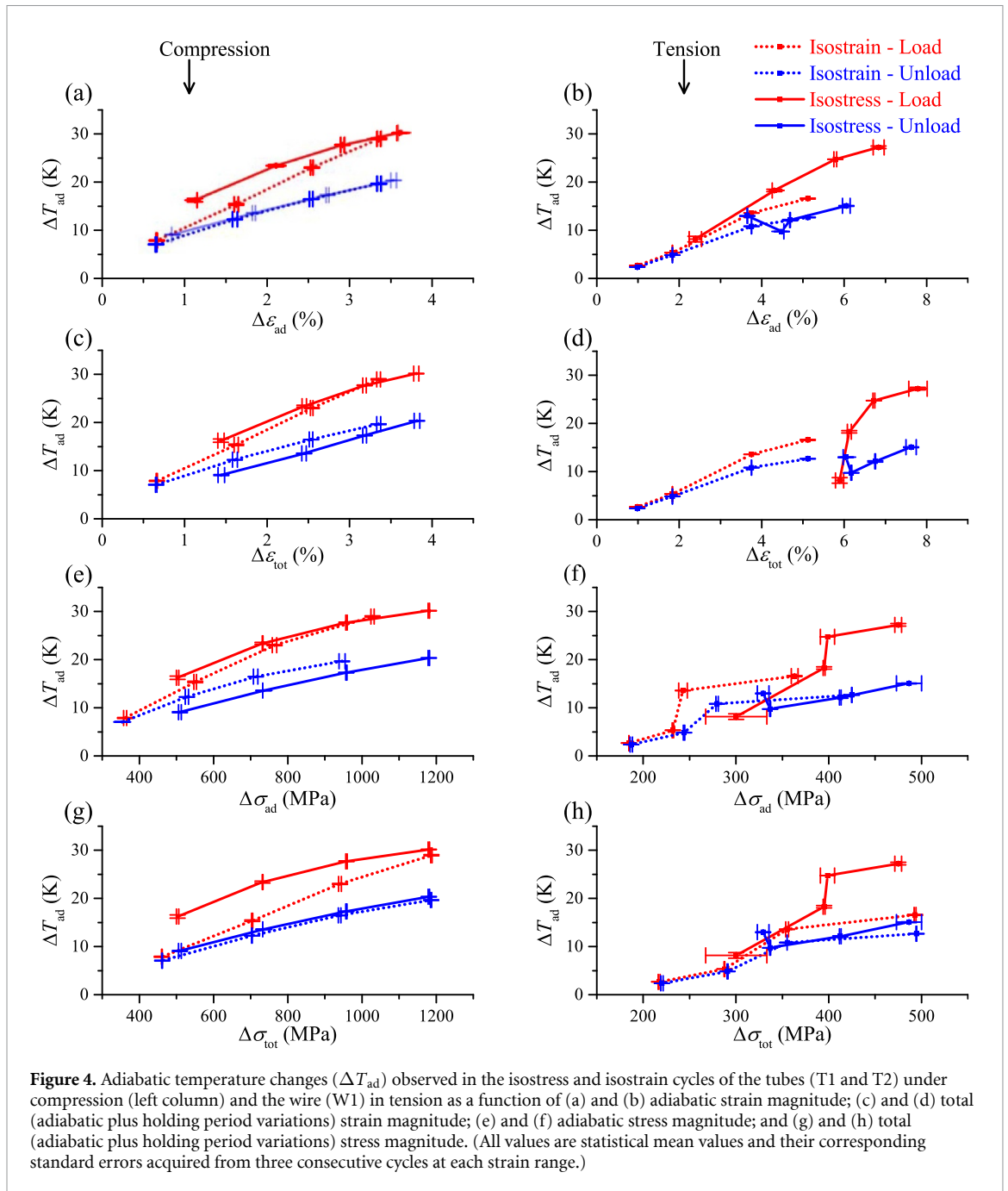
Figure 4 shows ΔT_{ad} generated by the isostress and isostrain cycles as a function of the total stress/strain ($\Delta\sigma_{\text{tot}}$, $\Delta\varepsilon_{\text{tot}}$) and adiabatic stress/strain ($\Delta\sigma_{\text{ad}}$, $\Delta\varepsilon_{\text{ad}}$). It should be noted that $\Delta\varepsilon_{\text{ad}}$ and $\Delta\sigma_{\text{ad}}$ show the variations that occur only during the adiabatic loading/unloading segment of each cycle and $\Delta\varepsilon_{\text{tot}}$ and $\Delta\sigma_{\text{tot}}$ include the stress/strain variations during the holding period of the cycles as well. In isostress cycles with constant stress during the holding period, $\Delta\sigma_{\text{tot}}$ is equal to $\Delta\sigma_{\text{ad}}$ (same data points). Similarly, in isostrain cycles $\Delta\varepsilon_{\text{tot}}$ is equal to $\Delta\varepsilon_{\text{ad}}$ (same data points). The data points are the statistical means and standard errors acquired from three consecutive cycles for each $\Delta\varepsilon$. Since the condition of the samples during the first adiabatic unloading after the quasi-isothermal loading is different to the rest of the adiabatic loading/unloading segments (see temperature-time profiles in figure 3), ΔT_{ad} of the first unloading is not included in the mean value calculations.

It is important to note that, as table 1 shows, to avoid exerting negative stress on the thin wire and to prevent it from bending during the unloading, the designated unloading strain limits of the wire are relatively large (identical for $\Delta\varepsilon_3$ and $\Delta\varepsilon_4$) compared to those of the tubes. Consequently, smaller reverse transformation and ΔT_{ad} occur in the wire upon unloading. This is the reason for the non-monotonic trend of unloading ΔT_{ad} for the wire under tension observed in figure 4, where the unloading ΔT_{ad} for the smallest strain range ($\Delta\varepsilon_1$) is larger than that of the second-smallest strain range ($\Delta\varepsilon_2$); compare figure 3(b) with figure A.2 of appendix A, supplementary materials. As will be discussed later (section 3.3.2), these non-monotonic trends become monotonic once the additional transformation and the heat release/absorption during the holding period are accounted for.

In all cases, ΔT_{ad} increases with both $\Delta\varepsilon_{\text{ad}}/\Delta\sigma_{\text{ad}}$ and $\Delta\varepsilon_{\text{tot}}/\Delta\sigma_{\text{tot}}$ since the magnitude of the transformation increases with the applied stress/strain range. Because of the flat plateau and large additional transformation during the holding period, the difference between the isostress and isostrain cycles is more pronounced in tension. As evidenced by figure 4, generating the same ΔT_{ad} under tension requires lower stresses and larger strains compared to compression (due to tension-compression asymmetry). It is interesting to note (see figures 4 (f) and (h)) that in the case of tension there is a significant increase in ΔT_{ad} at around 400 MPa for isostress cycles and at around 250 MPa for isostrain cycles, which corresponds to the beginning of the flat transformation plateau in tension (see figure 3(f)). Compared to isostrain cycles, in isostress cycles, the transformation plateau effectively occurs at higher stresses because of the larger transformation that occurs and results in a more pronounced self-heating/cooling effect. Since the transformation plateau under compression is much steeper and the transformation occurs over wider stress ranges, this phenomenon is almost absent in the compression tests.

In compression, the largest ΔT_{ad} of 30.2 K for loading and 20.4 K for unloading are generated during the isostress cycle across $\Delta\varepsilon_4$ and $\Delta\sigma_{\text{ad/tot}}$ of 1200 MPa. In tension, the largest ΔT_{ad} of 27.2 K for loading and 15.1 K for unloading are also generated during the isostress cycles across $\Delta\varepsilon_4$ but with $\Delta\sigma_{\text{ad/tot}}$ of only around 480 MPa, which is more than 48% lower than the $\Delta\sigma_{\text{ad/tot}}$ of 935 MPa that can generate similar ΔT_{ad} in compression. The difference between $\Delta\varepsilon_{\text{ad}}$ and $\Delta\varepsilon_{\text{tot}}$ (in the isostress cycles) is much larger in tension than in compression because, as a consequence of the flat plateau of tension, the majority of the transformation in smaller $\Delta\varepsilon$ ranges occurs throughout the holding period rather than the adiabatic loading/unloading segment. Note that these adiabatic temperature changes are directly observed and the corrected adiabatic temperature changes are even larger, as discussed in section 3.3.2.

With respect to the stress magnitude, an isostress cycle can generate significantly higher adiabatic temperature changes at considerably lower stress magnitudes in both compression and tension. In compression, with around 500 MPa of $\Delta\sigma_{\text{tot}}$, the isostress cycle generates ΔT_{ad} of 16.2 and 9.1 K for loading



and unloading, respectively, while the isostrain cycle generates only 9.2 and 8.0 K in loading and unloading, respectively. Because of the flat plateau and larger additional transformation throughout the holding period, this difference is significantly more pronounced in tension. Indeed, with $\Delta\sigma_{tot}$ of even slightly lower than 500 MPa, isostress cycle in tension generates 27.2 and 15.1 K for loading and unloading, respectively, while the isostrain cycle generates only 16.6 and 12.7 K for loading and unloading, respectively. Generating large ΔT_{ad} in lower $\Delta\sigma_{tot/ad}$ is the key superiority of an isostress cycle, especially for practical applications where the maximum applicable stress is limited by structural, functional and/or operational factors. It should be noted that, as will be shown later (sections 3.3.2 and 3.4), the additional non-adiabatic transformation and entropy change in an isostress cycle, which are not considered in ΔT_{ad} shown in this section, further boosts the cooling/heating performance of such a cycle.

Temperature (transformation) irreversibility, which is caused by hysteresis losses and is observed to be the difference between the loading and unloading ΔT_{ad} , has different trends in the isostress cycle with complete transformation (the maximum that can be achieved under a given stress/strain) and the isostrain cycles with constrained transformation. Accordingly, the temperature irreversibility is larger and almost constant in the isostress cycles (loading and unloading ΔT_{ad} lines are almost parallel in the isostress). This is

clearly visible in compression (figure 4), but not in tension due to the relatively large minimum unloading strain upon unloading, as discussed above. In contrast, in isostrain cycles, the irreversibility increases with the applied strain range ($\Delta\varepsilon_{\text{ad}/\text{tot}}$) since the magnitude of the transformation increases (loading and unloading ΔT_{ad} lines are not parallel). Therefore, when $\Delta\varepsilon_{\text{ad}}$ approaches $\Delta\varepsilon_{\text{max}}$, as expected, the difference between the isostrain and isostress cycles becomes less pronounced, although it does not disappear entirely (the temperature irreversibility of the isostrain is equal to that of the isostress).

3.3.2. Coefficient of performance

Although COP is more meaningful for devices, to evaluate and compare the elastocaloric performance of different materials, a variant of it, that is COP_{mat} , has been used extensively in the literature. Different methods used for calculating the input work and subsequently COP_{mat} are presented in detail in [59, 66]. Using experimental data, COP_{mat} is typically calculated using equation (1) [13, 35, 45, 60]:

$$\text{COP}_{\text{mat}} = \rho \times c \times \frac{\Delta T_{\text{ad}}}{\oint \sigma d\varepsilon}. \quad (1)$$

For elastocaloric materials, COP_{mat} is the ratio between the generated thermal energy and the input mechanical energy. In equation (1), ρ is the density of the material and c is the specific heat capacity of the material. Due to experimental difficulties and computational complexities in determining the *in situ* variations in c and ρ during adiabatic loading/unloading, where the phase fraction, stress, strain and temperature all change, they are considered as constants with typical values of around 6500 kg m^{-3} for ρ and $430 \text{ J kg}^{-1} \text{ K}^{-1}$ for c [67–71]. Under adiabatic conditions, the enthalpy change ($c \times \Delta T_{\text{ad}}$) that manifests itself as ΔT_{ad} is usually considered equivalent to the latent heat of the stress-induced transformation. The denominator, which is the input mechanical energy, can be considered equal to the area under the stress–strain curve of the material that is significantly different in loading and unloading. With the widespread assumption that the energy released during the unloading segment (the area under the unloading curve in the stress–strain diagram) is completely recovered, the hysteresis loop area (the area between the loading and unloading curves) is considered as the input mechanical energy of the elastocaloric cycle. It should be noted that achieving a hundred-percent energy recovery and having the dissipated/irrecoverable energy as the only input energy is questionable in practice, especially in a real device that inevitably has multiple other losses [43]. As a consequence of all of the abovementioned issues, COP_{mat} should be considered as an idealized notion that solely considers the material and consequently should not be compared directly with COP of an actual cooling/heat-pumping system (e.g. an actual vapor-compression system).

In the current form of COP_{mat} , the only variable that represents the heating/cooling energy is ΔT_{ad} . Nevertheless, in an isostress cycle, a considerable portion of the latent heat is released/absorbed non-adiabatically as a consequence of the ongoing transformation during the holding period. The negative effect of this additional non-adiabatic heating/cooling energy, which is the significantly larger hysteresis loop area, is considered in the input energy part of the COP_{mat} but its positive effect, which is the increased entropy change and enhanced cooling/heating energy, is not reflected in ΔT_{ad} . Therefore, a one-to-one comparison between the COP_{mat} of the isostress and isostrain cycles would be inaccurate and misleading. To capture this additional non-adiabatic heating/cooling experimentally, a modified isostrain cycle, named S-comp cycle, with two adiabatic loadings and two adiabatic unloading segments per cycle was applied to T2 in compression (with respect to $\Delta\varepsilon_1$, $\Delta\varepsilon_2$ and $\Delta\varepsilon_3$ in table 1) and W1 in tension (with respect to all $\Delta\varepsilon$ in table 1). The aim of the second adiabatic loading and unloading segments is to capture the latent heat released/absorbed during the holding period of the isostress cycles through measurable adiabatic temperature changes. Since the enthalpy is a state function, it depends only on the initial and final conditions of the sample/environment and is not affected by the path that the system takes between the two points. Moreover, under adiabatic conditions, the enthalpy change that can be considered equal to the latent heat release/absorption is manifested through ΔT_{ad} . Therefore, if the stress–strain changes that occur during the holding period of an isostress cycle can be reproduced adiabatically, an additional ΔT_{ad} can be measured and used to assess the enthalpy change resulting from the additional transformation during the holding period.

Figure 5 shows the results of applying S-comp cycles in tension and compression across the smallest strain range ($\Delta\varepsilon_1$). In the S-comp cycles, the initial quasi-isothermal loading (dashed magenta lines in figures 5(a)–(d)) and the first adiabatic unloading that follows it (dotted black lines in figures 5(a)–(d)) are identical to the normal isostrain cycles of the same strain range ($\Delta\varepsilon_1$ in the case of figure 5). The final strain of the second adiabatic unloading (dotted blue lines in figures 5(a)–(d)) is equal to the strain that the isostress cycle of the same strain range ($\Delta\varepsilon_1$ in the case of figure 5) reaches at the end of its constant-stress holding period. The strain limits of the subsequent adiabatic loading/unloading (solid black and blue lines in figures 5(a) and (b)) are determined in the same way. Consequently, the total strain range ($\Delta\varepsilon_{\text{tot}}$) covered by the two adiabatic parts of the S-comp loading/unloading for each strain range is equal to $\Delta\varepsilon_{\text{tot}}$ of the

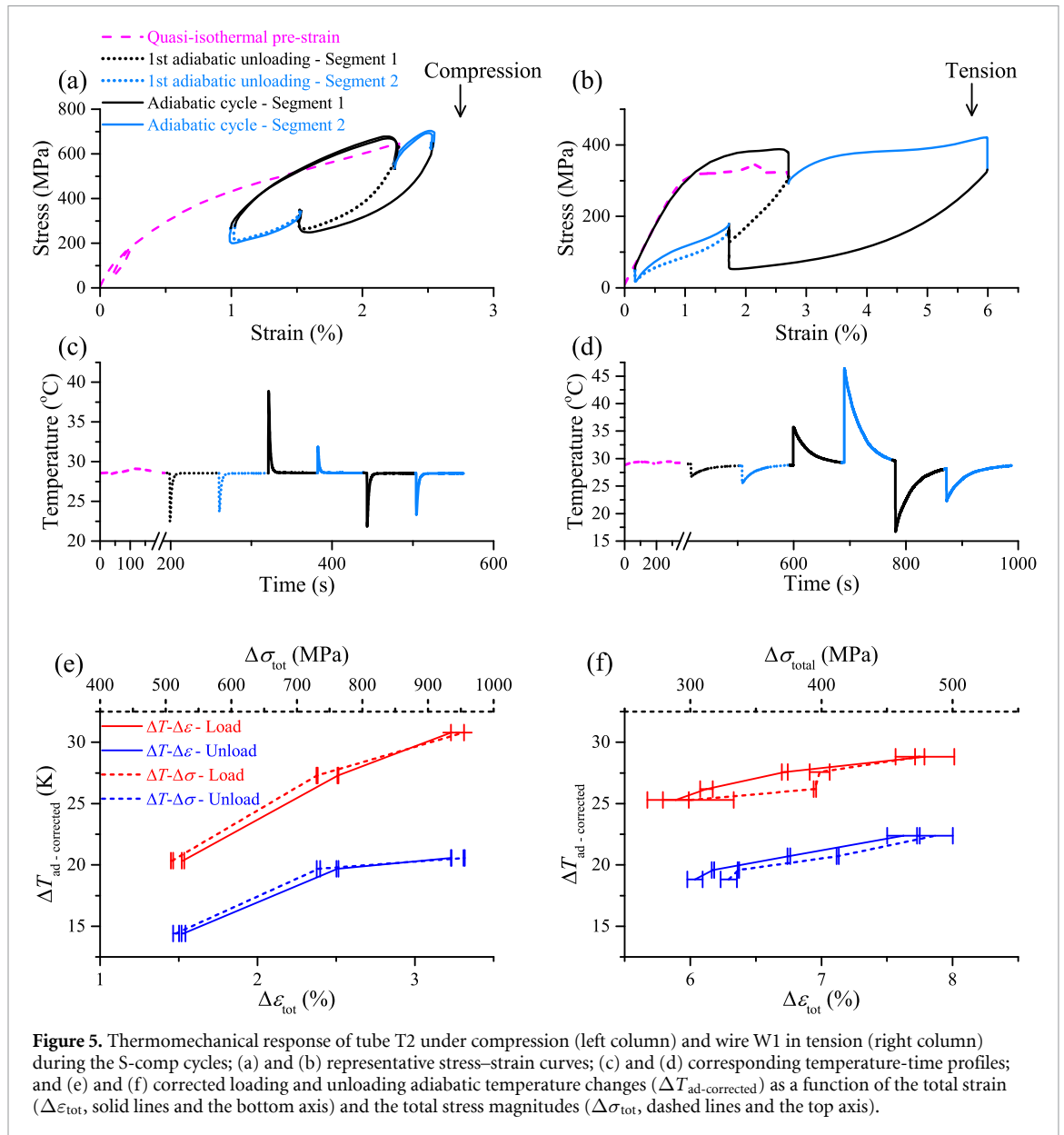
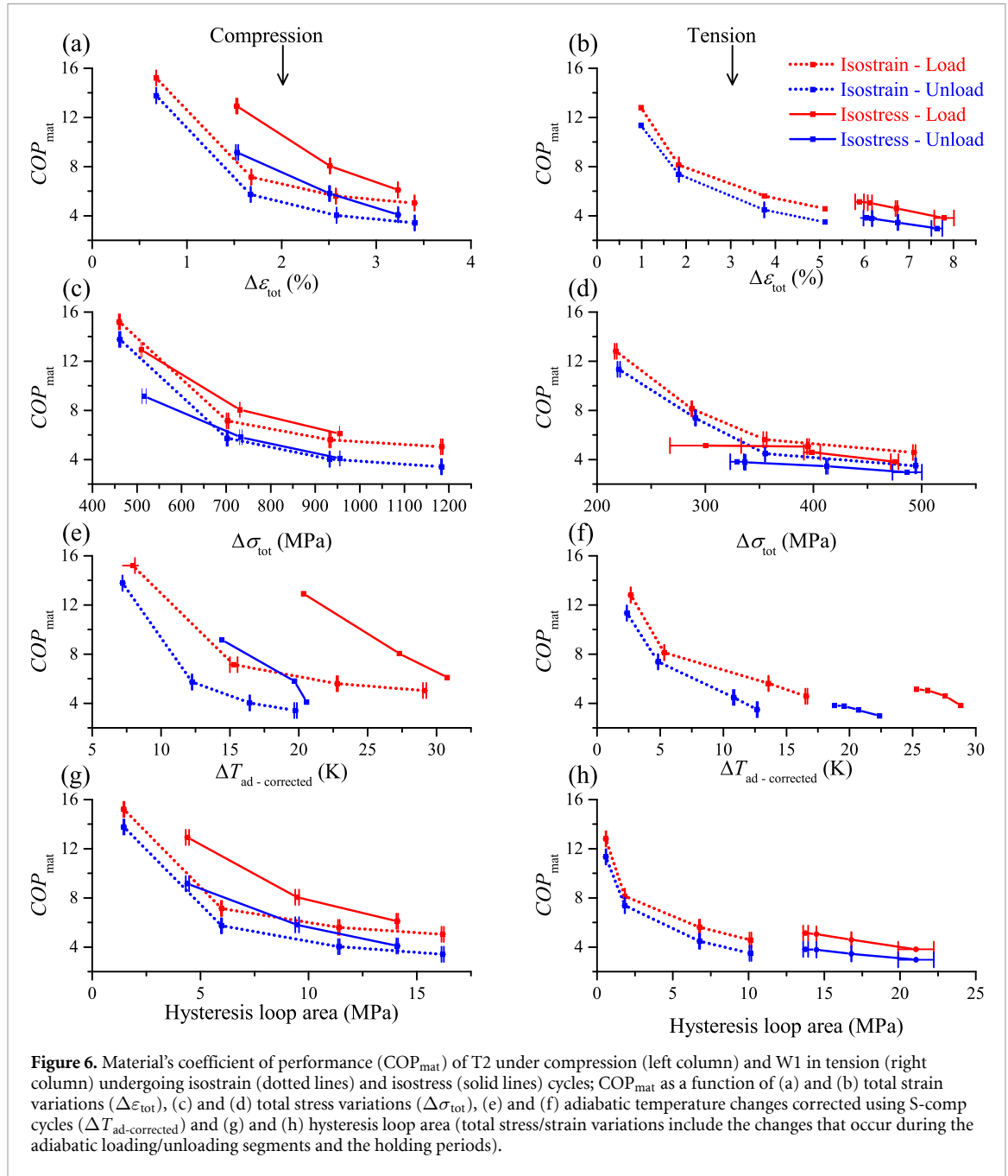


Figure 5. Thermomechanical response of tube T2 under compression (left column) and wire W1 in tension (right column) during the S-comp cycles; (a) and (b) representative stress–strain curves; (c) and (d) corresponding temperature–time profiles; and (e) and (f) corrected loading and unloading adiabatic temperature changes ($\Delta T_{ad-corrected}$) as a function of the total strain ($\Delta \varepsilon_{tot}$, solid lines and the bottom axis) and the total stress magnitudes ($\Delta \sigma_{tot}$, dashed lines and the top axis).

corresponding isostress cycle. The additional ΔT_{ad} measured from the second adiabatic loading/unloading of the S-comp cycles is added to the ΔT_{ad} of the corresponding isostress cycles (shown in figure 4), and a corrected ΔT_{ad} ($\Delta T_{ad-corrected}$ shown in figures 5(e) and (f)) is used to calculate the COP_{mat} values shown in figure 6. Once the adiabatic temperature changes are corrected, the benefits of the isostress cycles are better understood. In tension, applying around 480 MPa of stress generates $\Delta T_{ad-corrected}$ of 28.9 and 22.4 K for loading and unloading. In compression, applying around 955 MPa of stress generates $\Delta T_{ad-corrected}$ of 30.8 and 20.6 K for loading and unloading.

Although the S-comp cycle is a good (or perhaps the best) experimentally feasible method for estimating the additional heating/cooling during the holding period of isostress cycles, it is not completely accurate. The reason is that although state functions depend only on the initial and final states of the sample/environment, the state of a sample (phase fraction–temperature or stress–strain–temperature combination) at the end of the holding period of an isostress cycle is similar but not identical to its state at the end of the second adiabatic loading/unloading segment of its corresponding S-comp cycle. The reason is that, throughout the holding period of an isostress cycle, the stress is constant, and there is no considerable self-heating/cooling as the transformation freely progresses towards its final equilibrium state. In contrast, the equivalent S-comp cycle has two adiabatic segments, both with considerable self-heating/cooling and constrained strains during the holding periods, both of which suppress the transformation. As a result, compared to the holding period of an isostress cycle, the second adiabatic loading of the equivalent S-comp cycle generates higher/lower



stresses and somewhat smaller latent heat release/absorption. This means that the $\Delta T_{ad-corrected}$ might underestimate the total latent heat released/absorbed by the isostress cycle. Considering these limitations, a phenomenological model, capable of capturing the entropy changes under non-adiabatic conditions, was used to thoroughly understand the fundamental differences between the isostrain and isostress cycles (see section 3.4).

Figure 6 shows that in both tension and compression, the COP_{mat} decreases as the magnitude of the transformation and consequently $\Delta\varepsilon$, $\Delta\sigma$, ΔT_{ad} and the hysteresis loop area increase. Paradoxically, this implies that by avoiding the transformation that generates the elastocaloric effect (reducing $\Delta\varepsilon$, $\Delta\sigma$, ΔT_{ad} and the hysteresis loop area), the elastocaloric efficiency of the material improves significantly. Similar trends of a decrease in the COP_{mat} with increasing the applied strain were previously shown in [26]. The hysteresis loop area has the dominant effect, and maximizing ΔT_{ad} and COP_{mat} at the same time is not feasible. Therefore, a compromise should be made between the two to achieve the optimum outcome. Decreasing the magnitude of the transformation or suppressing it, for instance, by decreasing the grain size down to the nanoscale [50, 51], significantly decreasing the sample size to induce structure–microstructure interactions [52] or having a large volume of non-transformable precipitations in the sample [72], would decrease the

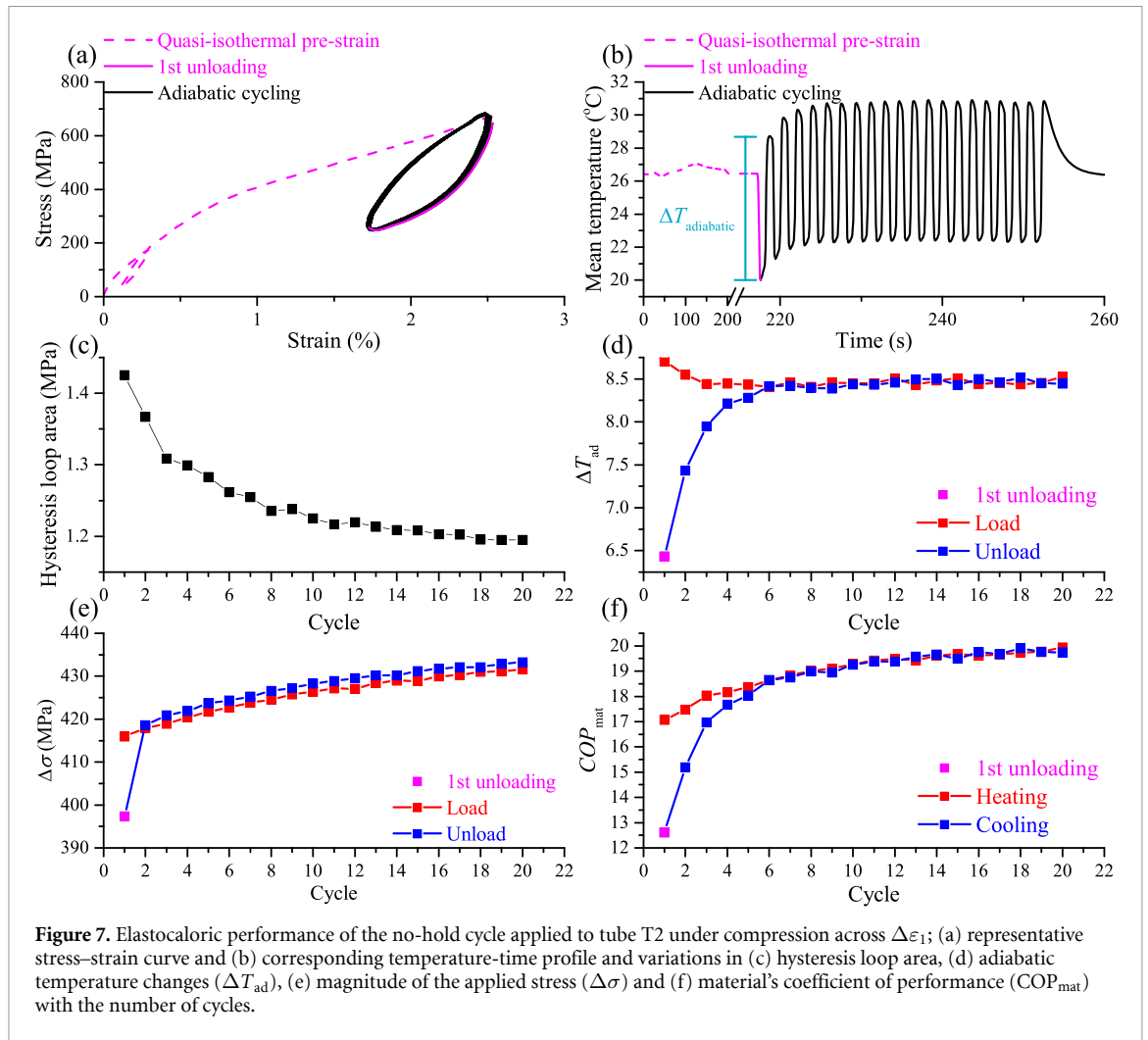
hysteresis loop area and increase the COP_{mat} . However, doing so decreases the adiabatic temperature changes and the cooling/heating energy as well. As shown in figure 6, the maximum COP_{mat} values of 15.2 and 13.8 for heating and cooling in compression and 12.8 and 11.3 for heating and cooling in tension are achieved in the minimum applied stress/strain ranges that correspond to the minimum phase transformation magnitude and minimum ΔT_{ad} . As the applied stress/strain and the magnitude of the transformation increase, the isostress cycles outperform the isostrain cycles by offering the best combination of $\Delta\sigma_{tot}$, ΔT_{ad} and hysteresis loop areas in both tension and compression. Due to the complete phase transformation and equilibrium phase fraction in isostress cycles, the COP_{mat} values are less affected by variations in the applied stress/strain ranges. Because of the flat transformation plateau, the stability of the COP_{mat} values is more evident in tension. The stability of the COP_{mat} values indicates that the isostress cycles can fully exploit the phase transformation in small stress ranges, which is highly beneficial for practical applications and devices where the applicable stress/strain range is a limiting factor. The flat plateau in tension results in a considerably large additional non-adiabatic transformation in the isostress cycles that in turn drastically increases the hysteresis loop area and therefore decreases the COP_{mat} values. It is interesting to note that the best performance in terms of COP_{mat} and ΔT_{ad} (figure 6(e)), maximization of which is highly desirable in practical devices, is demonstrated by the isostress cycle in compression, which compared to the isostress cycle in tension, has a significantly smaller hysteresis loop area (see figures 6(g) and (h)) in similar ΔT_{ad} .

3.3.3. No-hold cycles

One type of elastocaloric cycle (named the no-hold cycle here) that is sometimes reported in the literature [16, 17] is a no-hold cycle. Applying this cycle excludes the time (period) required for heat transfer after loading/unloading segments, meaning that the most of the released/absorbed latent heat from the elastocaloric effect cannot be transferred to/from the heat sink/source and the cooling/heating power is essentially zero (in particular if loading/unloading is performed under adiabatic conditions). Accordingly, the hysteresis loop area is significantly reduced since there is no stress/strain decrease/increase as the hysteresis related to the thermodynamic work required to pump the heat from the heat sink to the heat source (or vice versa) is excluded and only the hysteresis of the material itself is included. As figure 7 shows, when the holding period is omitted from an elastocaloric cycle, the self-heating/cooling effect of each cycle accumulates. Thus, the transformation is suppressed and the hysteresis loop area is further decreased. Under these circumstances, practically nonrealistic and superficially high COP_{mat} values are obtained.

Figure 7 summarizes the thermal and mechanical behavior of T2 undergoing 20 consecutive no-hold cycles (specifications are listed in table 1) across $\Delta\varepsilon_1$ (see appendix A, supplementary material—figures A.3 and A.4 for the data of other strain ranges). Figure 7(a) shows the stress–strain response and figure 7(b) shows the corresponding temperature–time profile. Figures 7(c), (d), (e) and (f), respectively, show variations in the hysteresis loop area, ΔT_{ad} , the stress magnitudes and COP_{mat} with the number of loading/unloading cycles. Some of the fundamental problems of the no-hold cycle will be discussed here. The first issue is calculating the adiabatic temperature changes since it is not clear which temperature changes should be considered as the adiabatic temperature changes of the elastocaloric effect. Typically, the differences between the temperature peaks generated by the material (minimum and maximum of each cycle as indicated by ΔT_{ad} in figure 7(b)) are considered as ΔT_{ad} [16, 17]. It should be noted that this definition is not applicable to the very first unloading, where the maximum temperature is the ambient temperature and is not generated by the material (as indicated by the solid magenta line in figure 7(b)). The parameters of the first unloading are denoted by magenta data points in figures 7(d)–(f). It is observed that in the absence of a holding period, accumulation of hysteresis heat losses shifts both minimum and maximum temperatures up and suppresses the forward exothermic transformation. Consequently, at the beginning and before ultimately stabilizing, the loading adiabatic temperature changes decrease, while the unloading adiabatic temperature changes increase (see figure 7(d)). Moreover, the hysteresis loop area decreases and the stress range required to reach the fixed strain range ($\Delta\varepsilon_1$ in the case of figure 7) increases in each cycle as a consequence of the transformation suppression. As can be observed in figure 7(f), despite the fact that ΔT_{ad} stabilizes after a certain number of cycles (figure 7(d)), since the hysteresis has the dominant effect on COP_{mat} and considering the fact that it keeps decreasing (figure 7(c)), COP_{mat} increases with cycling and reaches 19.95 for heating and 19.75 for cooling in the last cycle.

By definition, under the adiabatic conditions thus established, there is no thermal interaction between the sample and the environment that in turn means that the input energy, assumed equal to the hysteresis loop area, is solely used to heat up and cool down the sample itself rather than doing any actual thermal work on the environment. Therefore, despite the fact that COP_{mat} values of no-hold cycles are considerably higher because of the decreasing hysteresis loop area, zero thermodynamic work and suppressed transformation, they do not reflect the capability of the material to do thermal work and therefore result in nearly zero

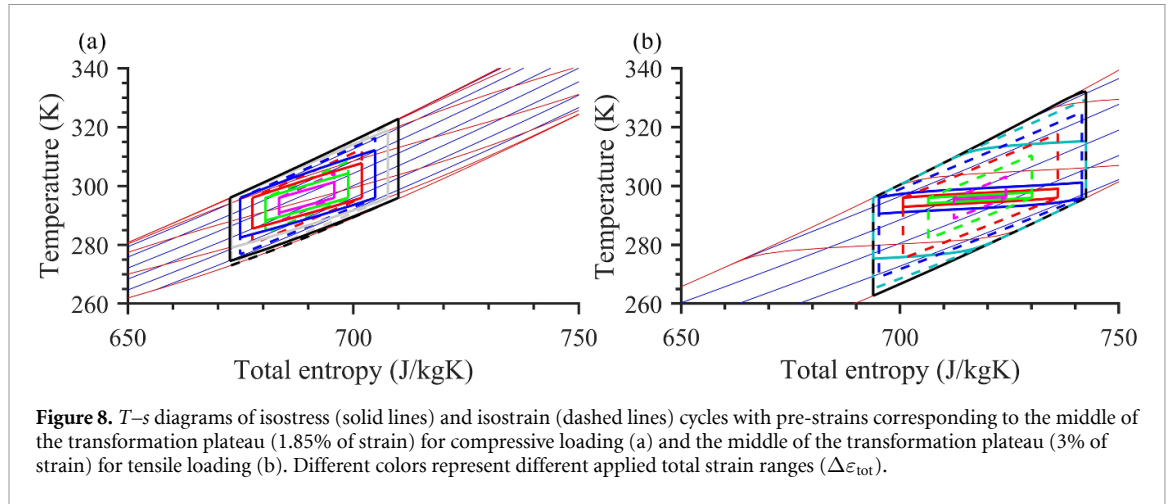


cooling/heating power. Moreover, although instantaneous heat transfer is not theoretically impossible, in an actual elastocaloric device, a holding period is required so that the generated/absorbed heat can be transferred to the heat transfer fluid or the contact heat sink/source. Therefore, no-hold cycles cannot be utilized in actual elastocaloric applications despite having superficially high COP_{mat} values. On the other hand, it is possible to use an Ericsson thermodynamic cycle in which the heat transfer occurs during the slower loading/unloading and the sample maintains isothermal conditions [59]. Nevertheless, since adiabatic temperature changes are not generated under such circumstances, equation (1) cannot be used for COP_{mat} calculations.

3.4. Elastocaloric performance of the material under different thermodynamic cycles—phenomenological modeling results

To capture the cooling/heating performance of the isostress and isostrain cycles in compression and tension, theoretical analysis was performed as well. Similar to the isostress/isostrain experiments, the simulated cycles include four basic operational steps: loading (elastocaloric effect heats up the material), holding the stress/strain constant (material cools down back to the ambient temperature), unloading (elastocaloric effect cools down the material), holding the stress/strain constant (material heats up back to ambient temperature). In the simulations, both the isostress and isostrain cycles have a constant total entropy change (identical $\Delta\varepsilon_{tot}$) and therefore a similar cooling energy. Similar to the experiments, different $\Delta\varepsilon$ ranges with pre-straining to the middle of the transformation plateau were applied to each cycle.

The cycles were compared with respect to ΔT_{ad} , specific cooling (q_c) and heating (q_h) energy and the cooling and heating COP_{mat} values (COP_{mat-c} and COP_{mat-h}). Using the T - s diagram, q_h is defined as the area under the upper iso-field line (equation (2)), while q_c is defined as the area under the lower iso-field line (equation (3)). The difference between the specific heating and the cooling energy is the input energy (w ,



equation (4)), while the ratio between q_h and q_c ; and w is defined as $\text{COP}_{\text{mat-h}}$ (equation (5)) and $\text{COP}_{\text{mat-c}}$ (equation (6)), respectively:

$$q_h = \int_{\text{high field}} T ds, \quad (2)$$

$$q_c = \int_{\text{low field}} T ds, \quad (3)$$

$$w = q_h - q_c, \quad (4)$$

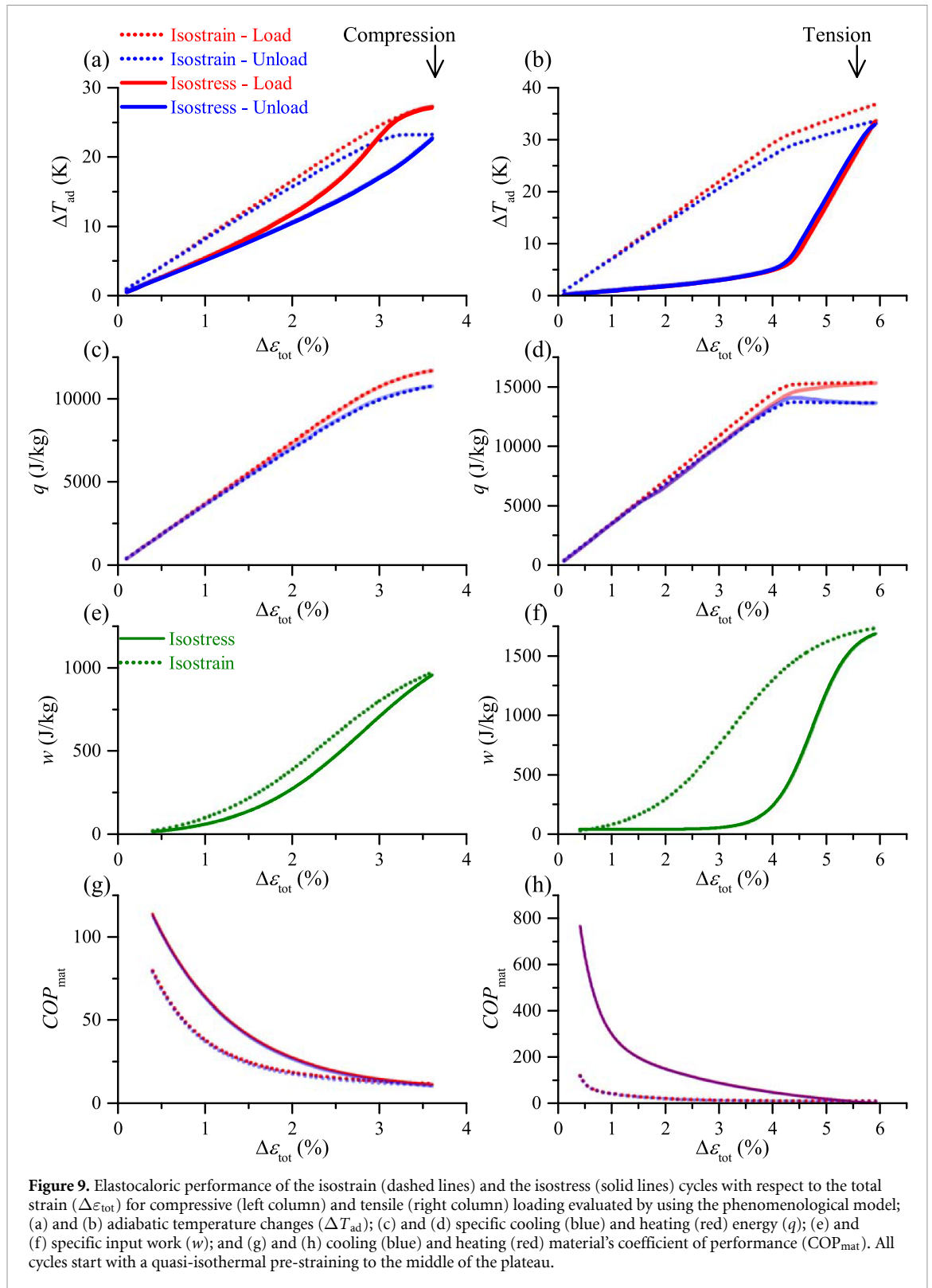
$$\text{COP}_{\text{mat-h}} = \frac{q_h}{w}, \quad (5)$$

$$\text{COP}_{\text{mat-c}} = \frac{q_c}{w}. \quad (6)$$

Figure 8 shows the thermodynamic cycles in the T - s diagrams under fixed total strain conditions for compressive and tensile loading (different colors represent different applied total strain ranges). It is observed that the isostress and isostrain cycles generate different ΔT_{ad} when the entropy change is constant (fixed $\Delta\varepsilon_{\text{tot}}$). As previously explained, the strain does not change during the isostrain holding period, while during the isostress holding period, the strain increases (when the sample is cooling down after being loaded) or decreases (when the sample is heating up after being unloaded). Therefore, in order to have identical $\Delta\varepsilon_{\text{tot}}$ in both cycles, the applied strain $\Delta\varepsilon_{\text{ad}}$ should be smaller in the case of the isostress cycle (where the rest of the strain is generated during the holding period), which results in a lower ΔT_{ad} for the isostress cycle, as also shown in figure 9(b). It is further evident that the difference between the isostress and isostrain cycles exists only in the cycles with partial transformation ($\Delta\varepsilon < \Delta\varepsilon_{\text{max}}$). If the applied stress/strain is large enough to induce a complete transformation, there would be no difference between the isostress and isostrain cycles, as already explained in the experimental results.

Compared to compression, the difference between the isostress and isostrain cycles is significantly more pronounced in tension (see figure 8). As explained earlier in the text, this is due to the almost entirely flat transformation plateau in tension, which results in almost flat isostress lines between zero and final stress/strain. Therefore, the entire entropy change at constant stress occurs in a very narrow temperature range. In compression, on the other hand, the sloped transformation plateau results in steeper isostress lines since the entropy change at constant stress occurs in a wider temperature range. Consequently, in tension and under isostress conditions, a small portion of the transformation occurs adiabatically and the majority of the transformation occurs throughout the holding period and during cooling/heating (approaching the ambient temperature). As can be seen in figure 8(b), the isostress tensile cycles in which most of the transformation occurs non-adiabatically during the holding period, are a good approximation of a Carnot cycle, which appears as a perfect rectangle in an T - s diagram and is theoretically the most efficient thermodynamic cycle since its input work is the minimum possible.

Figure 9 compares the performance of the isostrain and isostress cycles under compressive (left column) and tensile loading (right column). Since both the isostrain and isostress cycles were modeled at identical



$\Delta\varepsilon_{\text{tot}}$, which results in the same entropy change, the specific cooling and heating energies are similar for the isostrain and isostress cycles, as shown in figures 8(a) and 9(a). On the other hand, as already mentioned above, in the case of the isostress cycles, the initial part of the transformation occurs adiabatically, while the second part occurs non-adiabatically during the holding period. As a consequence, the adiabatic temperature changes of the isostress cycles are smaller than those of the isostrain cycles (for the same applied strain). This is more pronounced in tension, where ΔT_{ad} is only up to 5 K in the isostress cycle when the total strain is limited to about 4%. At large strains with a more complete transformation, ΔT_{ad} increases and reaches that of the isostrain cycle at complete transformation (around 6% of strain). The major and most important

difference between the isostrain and isostress cycle is in the input energy that is significantly smaller in the isostress cycle since the enclosed area of the thermodynamic cycle in the T - s diagram of the isostress cycle is smaller than that of the isostrain cycle. Consequently, as shown in figures 9(g) and (h), the isostress cycle generates larger COP_{mat} values than the isostrain cycle, which is significantly more pronounced in tension, where at small and moderate strains, the cycle approaches the Carnot thermodynamic cycle. For compression and moderate strains, using the isostress instead of the isostrain cycle can improve COP_{mat} by up to 50%, while in the case of a complete transformation, the COP_{mat} values for both cycles would be the same and close to 10 (see figure 8(g)). On the other hand, in the case of tensile loading and moderate strains, where the cycle approaches the Carnot cycle, the COP_{mat} values of the isostress cycle are much larger compared to the isostrain cycle (even 500% larger at strains of up to 4%). Once the strain is large enough to cover the entire transformation plateau, both cycles show the same performance under tensile loading as well.

As already mentioned in the Materials and Methods section, a direct comparison between the experimental and modeling results is not possible because the model that is used for the simulations does not account for the hysteresis losses of the elastocaloric material. The modeling results indicate a potentially huge improvement in the efficiency by using isostress cycles, particularly for tensile loading. Nevertheless, as observed in the experiments, a smaller improvement could be achieved in reality because of the significant hysteresis losses. From a theoretical point of view, it can be concluded that the isostress cycles are especially interesting for elastocaloric materials with a rather flat transformation plateau (tensile loading) and a small(er) hysteresis (e.g. Ni-Ti-Cu or Cu-based alloys have smaller hysteresis losses compared to binary Ni-Ti alloys [45, 73–75]), where there would be the most significant improvement in efficiency. It should be noted that, according to the experimental results, the isostress cycle is more beneficial for compressive loading than tensile loading. Since the hysteresis loop area, which has the predominant effect in COP_{mat} calculations, is significantly larger in tensile isostress cycles, the theoretical and experimental analyses lead to different conclusions.

4. Conclusion

Using commercially available superelastic thin-walled NiTi tubes for compression and a thin NiTi wire for tension, different thermodynamic cycles were studied experimentally and theoretically with an emphasis on the parameters of the holding period. The cycles were applied to the samples across multiple stress/strain ranges at room temperature with constant stress throughout the holding periods (isostress cycles), constant strain throughout the holding periods (isostrain cycles) and with no holding periods (no-hold cycles). The results revealed that the applied thermodynamic cycle significantly affects the thermomechanical response and thus the cooling/heating efficiency of the material. A Carnot-like thermodynamic cycle with enhanced heating/cooling efficiency can be generated by applying isostress cycles and partial transformation. Large reproducible (directly measured and repeatable in trained samples and in consecutive cycles without degradation) adiabatic temperature changes of up to 30.2 K upon loading and 20.4 K upon unloading in tubes and 27.2 K upon loading and 15.1 K upon unloading in the wire can be generated using isostress cycles and commercially available NiTi. The observed adiabatic temperature changes are among the largest reproducible adiabatic temperature changes directly measured in any caloric material.

In addition to improving the efficiency (COP_{mat}), one of the most important findings of this work is that using the isostress cycle allows for generating larger adiabatic temperature changes at smaller stress levels. From the application point of view, it is worth mentioning that medium- and large-scale elastocaloric devices (e.g. based on an active elastocaloric regenerator [35]) are made out of multiple elastocaloric elements, such as thin-walled tubes under compression or thin sheets or wires under tension. Longer elastocaloric elements are expected to improve the performance of an active elastocaloric regenerator. However, the maximum stress that can be applied to the tubes must be below the critical buckling stress, which itself decreases significantly with increasing the length of the tubes [26]. Consequently, the large stress magnitude that can induce a complete transformation and generate high adiabatic temperature changes cannot be applied to long tubes. Although length is not a major concern for thin sheets and wires under tension in the absence of buckling, the larger the applied stress is, the shorter the fatigue life would be, which is the main bottleneck of tensile loading. Along with several other studies [25, 76, 77], our previous studies have shown that the tensile fatigue life can be significantly improved when smaller stress magnitudes are applied and a partial phase transformation occurs [25]. Therefore, by utilizing isostress cycles rather than isostrain cycles, the applied stress can be decreased, while a large transformation is induced. Moreover, in an active regenerator configuration [35], ideally, hundreds of elastocaloric elements need to be simultaneously loaded. Hence, the significantly increased total cross-sectional area requires considerably large forces to induce the martensitic transformation. This means that heavy-duty bulky actuators are required that would increase the size and cost of the final device. Thus, isostress cycles, which allow for generating relatively large temperature changes

under smaller applied stresses, can be utilized in active regenerators not only to enhance the tensile fatigue life and increase the durability, but also to increase the number of elastocaloric elements and increase the overall cooling or heat-pumping characteristics or decrease the required force and size of the driver.

Data availability statement

All data that support the findings of this study are included within the article (and any supplementary files).

Acknowledgments

This work was supported by the European Research Council under the Horizon 2020 program (ERC Starting Grant No. 803669). Jaka Tušek gratefully acknowledges the support of the Slovenian Research Agency (ARRS Research Core Funding No. P2-0422).

Credit authorship contribution statement

Parham Kabirifar: Conceptualization, Methodology, Investigation, Formal analysis, Validation, Visualization, Writing—Original Draft; Jonas Trojer: Investigation, Writing—Review & Editing; Miha Brojan: Resources, Writing—Review & Editing; Jaka Tušek: Conceptualization, Software, Resources, Supervision, Funding acquisition, Writing—Review & Editing.

Conflict of interest

The authors declare that they have no known competing financial interests or personal relationships that could have appeared to influence the work reported in this paper.

ORCID iDs

Parham Kabirifar  <https://orcid.org/0000-0002-4570-7881>

Jonas Trojer  <https://orcid.org/0000-0002-7040-1569>

Miha Brojan  <https://orcid.org/0000-0002-3342-9562>

Jaka Tušek  <https://orcid.org/0000-0003-3262-9244>

References

- [1] McLinden M O, Brown J S, Brignoli R, Kazakov A F and Domanski P A 2017 Limited options for low-global-warming-potential refrigerants *Nat. Commun.* **8** 14476
- [2] Ciconkov R 2018 Refrigerants: there is still no vision for sustainable solutions *Int. J. Refrig.* **86** 441–8
- [3] Jia L, Jin W and Zhang Y 2017 Experimental study on R32 leakage and diffusion characteristic of wall-mounted air conditioners under different operating conditions *Appl. Energy* **185** 2127–33
- [4] Cheong K W and Riffat S B 1996 Monitoring hydrofluorocarbon refrigerant leakage from air-conditioning systems in buildings *Appl. Energy* **53** 341–7
- [5] Ozone Secretariat 2020 *Handbook for the Montreal Protocol on Substances that Deplete the Ozone Layer* (Gigiri: Ozone Secretariat) (available at: <https://ozone.unep.org/sites/default/files/Handbooks/MP-Handbook-2020-English.pdf>)
- [6] Moya X and Mathur N D 2020 Caloric materials for cooling and heating *Science* **370** 797–803
- [7] Greco A, Aprea C, Maiorino A and Masselli C 2019 A review of the state of the art of solid-state caloric cooling processes at room-temperature before 2019 *Int. J. Refrig.* **106** 66–88
- [8] Trevizoli P V, Nakashima A T, Peixer G F and Barbosa J R 2017 Performance assessment of different porous matrix geometries for active magnetic regenerators *Appl. Energy* **187** 847–61
- [9] Labban O, Chen T, Ghoniem A F, Lienhard J H and Norford L K 2017 Next-generation HVAC: prospects for and limitations of desiccant and membrane-based dehumidification and cooling *Appl. Energy* **200** 330–46
- [10] US department of Energy 2014 *Energy Savings Potential and RD&D Opportunities for Non-Vapor-Compression HVAC Technologies* (<https://doi.org/10.2172/1220817>)
- [11] VHK and ARMINES 2016 *Preparatory Study: Commission Regulation (EC) No. 643/2009 with Regard to Ecodesign Requirements for Household Refrigeration Appliances and Commission Delegated Regulation (EU) No. 1060/2010 with Regard to Energy Labelling of Household Refrigeration*
- [12] Kabirifar P, Žerovnik A, Ahčin Ž, Porenta L, Brojan M and Tušek J 2019 Elastocaloric cooling: state-of-the-art and future challenges in designing regenerative elastocaloric devices *J. Mech. Eng.* **65** 615–30
- [13] Cui J, Wu Y, Muehlbauer J, Hwang Y, Radermacher R, Fackler S, Wuttig M and Takeuchi I 2012 Demonstration of high efficiency elastocaloric cooling with large ΔT using NiTi wires *Appl. Phys. Lett.* **101** 073904
- [14] Yang Z, Cong D, Yuan Y, Li R, Zheng H, Sun X, Nie Z, Ren Y and Wang Y 2020 Large room-temperature elastocaloric effect in a bulk polycrystalline Ni-Ti-Cu-Co alloy with low isothermal stress hysteresis *Appl. Mater. Today* **21** 100844
- [15] Tian X et al 2022 Accelerated design for elastocaloric performance in NiTi-based alloys through machine learning *J. Appl. Phys.* **131** 015104
- [16] Zhang K, Kang G and Sun Q 2019 High fatigue life and cooling efficiency of NiTi shape memory alloy under cyclic compression *Scr. Mater.* **159** 62–67

- [17] Lin H, Hua P and Sun Q 2022 Effects of grain size and partial amorphization on elastocaloric cooling performance of nanostructured NiTi *Scr. Mater.* **209** 114371
- [18] Xu S, Huang H-Y, Xie J, Takekawa S, Xu X, Omori T and Kainuma R 2016 Giant elastocaloric effect covering wide temperature range in columnar-grained Cu_{71.5}Al_{17.5}Mn₁₁ shape memory alloy *APL Mater.* **4** 106106
- [19] Mañosa L, Jarque-Farnos S, Vives E and Planes A 2013 Large temperature span and giant refrigerant capacity in elastocaloric Cu-Zn-Al shape memory alloys *Appl. Phys. Lett.* **103** 211904
- [20] Xiao F, Fukuda T and Kakeshita T 2013 Significant elastocaloric effect in a Fe-31.2Pd (at.%) single crystal *Appl. Phys. Lett.* **102** 161914
- [21] Hernández-Navarro F, Camarillo-García J-P, Aguilar-Ortiz C-O, Flores-Zúñiga H, Ríos D, González J-G and Álvarez-Alonso P 2018 The influence of texture on the reversible elastocaloric effect of a polycrystalline Ni₅₀Mn₃₂In₁₆Cr₂ alloy *Appl. Phys. Lett.* **112** 164101
- [22] Liu J, Zhao D and Li Y 2017 Exploring magnetic elastocaloric materials for solid-state cooling *Shape Mem. Superelasticity* **3** 192–8
- [23] Hou H, Cui J, Qian S, Catalini D, Hwang Y, Radermacher R and Takeuchi I 2018 Overcoming fatigue through compression for advanced elastocaloric cooling *MRS Bull.* **43** 285–90
- [24] Chluba C, Ossmer H, Zamponi C, Kohl M and Quandt E 2016 Ultra-low fatigue quaternary TiNi-based films for elastocaloric cooling *Shape Mem. Superelasticity* **2** 95–103
- [25] Tušek J, Žerovnik A, Čebren M, Brojan M, Žužek B, Engelbrecht K and Cadelli A 2018 Elastocaloric effect vs fatigue life: exploring the durability limits of Ni-Ti plates under pre-strain conditions for elastocaloric cooling *Acta Mater.* **150** 295–307
- [26] Porenta L, Kabirifar P, Žerovnik A, Čebren M, Žužek B, Dolenc M, Brojan M and Tušek J 2020 Thin-walled Ni-Ti tubes under compression: ideal candidates for efficient and fatigue-resistant elastocaloric cooling *Appl. Mater. Today* **20** 100712
- [27] Pieczyska E A, Tobushi H and Kulasinski K 2013 Development of transformation bands in TiNi SMA for various stress and strain rates studied by a fast and sensitive infrared camera *Smart Mater. Struct.* **22** 035007
- [28] Pieczyska E A, Gadaj S P, Nowacki W K and Tobushi H 2006 Phase-transformation fronts evolution for stress- and strain-controlled tension tests in TiNi shape memory alloy *Exp. Mech.* **46** 531–42
- [29] Ding L, Zhou Y, Xu Y, Dang P, Ding X, Sun J, Lookman T and Xue D 2021 Learning from superelasticity data to search for Ti-Ni alloys with large elastocaloric effect *Acta Mater.* **218** 117200
- [30] Cong D et al 2019 Colossal elastocaloric effect in ferroelastic Ni-Mn-Ti alloys *Phys. Rev. Lett.* **122** 255703
- [31] Qian S, Wang Y, Geng Y, Ling J, Muehlbauer J, Hwang Y, Radermacher R and Takeuchi I 2016 Experimental evaluation of a compressive elastocaloric cooling system *16th Int. Refrigeration and Air Conditioning Conf. at Purdue* vol 16 p 2385
- [32] Schmidt M, Schütze A and Seelecke S 2015 Scientific test setup for investigation of shape memory alloy based elastocaloric cooling processes *J. Refrig.* **54** 88–97
- [33] Bachmann N, Fitger A, Maier L M, Mahlke A, Schäfer-Welsen O, Koch T and Bartholomé K 2021 Long-term stable compressive elastocaloric cooling system with latent heat transfer *Commun. Phys.* **4** 1–6
- [34] Qian S, Wang Y, Xu S, Chen Y, Yuan L and Yu J 2021 Cascade utilization of low-grade thermal energy by coupled elastocaloric power and cooling cycle *Appl. Energy* **298** 117269
- [35] Tušek J, Engelbrecht K, Eriksen D, Dall'Olio S, Tušek J and Pryds N 2016 A regenerative elastocaloric heat pump *Nat. Energy* **1** 16134
- [36] Engelbrecht K, Tušek J, Eriksen D, Lei T, Lee C-Y, Tušek J and Pryds N 2017 A regenerative elastocaloric device: experimental results *J. Phys. D: Appl. Phys.* **50** 424006
- [37] Bruederlin F, Ossmer H, Wendler F, Miyazaki S and Kohl M 2017 SMA foil-based elastocaloric cooling: from material behavior to device engineering *J. Phys. D: Appl. Phys.* **50** 424003
- [38] Bruederlin F, Bumke L, Quandt E and Kohl M 2019 Cascaded SMA-film based elastocaloric cooling *2019 20th Int. Conf. on Solid-State Sensors, Actuators and Microsystems & EUROSENSORS XXXIII (TRANSDUCERS & EUROSENSORS XXXIII)* (IEEE) pp 1467–70
- [39] Ianniciello L, Bartholomé K, Fitger A and Engelbrecht K 2022 Long life elastocaloric regenerator operating under compression *Appl. Therm. Eng.* **202** 117838
- [40] Bruederlin F, Bumke L, Chluba C, Ossmer H, Quandt E and Kohl M 2018 Elastocaloric cooling on the miniature scale: a review on materials and device engineering *Energy Technol.* **6** 1588–604
- [41] Kirsch S M, Welsch F, Michaelis N, Schmidt M, Wiczorek A, Frenzel J, Eggeler G, Schütze A and Seelecke S 2018 NiTi-based elastocaloric cooling on the macroscale: from basic concepts to realization *Energy Technol.* **6** 1567–87
- [42] Greibich F et al 2021 Elastocaloric heat pump with specific cooling power of 20.9 W g⁻¹ exploiting snap-through instability and strain-induced crystallization *Nat. Energy* **6** 260–7
- [43] Hou H, Qian S and Takeuchi I 2022 Materials, physics and systems for multicaloric cooling *Nat. Rev. Mater.* **7** 633–52
- [44] Wollants P, Roos J R and Delaey L 1993 Thermally- and stress-induced thermoelastic martensitic transformations in the reference frame of equilibrium thermodynamics *Prog. Mater. Sci.* **37** 227–88
- [45] Tušek J, Engelbrecht K, Mañosa L, Vives E and Pryds N 2016 Understanding the thermodynamic properties of the elastocaloric effect through experimentation and modelling *Shape Mem. Superelasticity* **2** 317–29
- [46] Otsuka K and Ren X 2005 Physical metallurgy of Ti–Ni-based shape memory alloys *Prog. Mater. Sci.* **50** 511–678
- [47] Michaelis N, Schütze A, Welsch F, Kirsch S M and Seelecke S 2019 Novel experimental approach to determine elastocaloric latent heat *Shape Mem. Superelasticity* **5** 352–61
- [48] Chen H, Xiao F, Liang X, Li Z, Li Z, Jin X, Min N and Fukuda T 2019 Improvement of the stability of superelasticity and elastocaloric effect of a Ni-rich Ti-Ni alloy by precipitation and grain refinement *Scr. Mater.* **162** 230–4
- [49] Hou R, Xiao F, Li Z and Jin X 2022 The role of texture on superelasticity and elastocaloric effect in severely rolled Ti-44Ni-5Cu-1Al (at%) shape memory alloy *Scr. Mater.* **209** 114334
- [50] Kabirifar P, Li M and Sun Q 2019 Non-monotonic grain size dependence of phase transformation behavior in NiTi microscale samples *Scr. Mater.* **165** 50–54
- [51] Kabirifar P, Chu K, Ren F and Sun Q 2018 Effects of grain size on compressive behavior of NiTi polycrystalline superelastic macro- and micropillars *Mater. Lett.* **214** 53–55
- [52] Paul P P, Kabirifar P, Sun Q and Brinson L C 2019 Structure-microstructure interactions in compression deformation of NiTi shape memory alloy micropillars *Mater. Lett.* **257** 126693
- [53] Luo X H, Ren W J, Jin W and Zhang Z D 2017 Large elastocaloric effect in Ti-Ni shape memory alloy below austenite finish temperature *Chin. Phys. B* **26** 036501

- [54] Schmidt M, Schütze A and Seelecke S 2016 Elastocaloric cooling processes: the influence of material strain and strain rate on efficiency and temperature span *APL Mater.* **4** 064107
- [55] Tušek J, Engelbrecht K, Mikkelsen L P and Pryds N 2015 Elastocaloric effect of Ni-Ti wire for application in a cooling device *J. Appl. Phys.* **117** 124901
- [56] Gall K, Sehitoglu H, Chumlyakov Y I and Kireeva I V 1999 Tension–compression asymmetry of the stress–strain response in aged single crystal and polycrystalline NiTi *Acta Mater.* **47** 1203–17
- [57] Imran M and Zhang X 2020 Recent developments on the cyclic stability in elastocaloric materials *Mater. Des.* **195** 109030
- [58] Qian S, Geng Y, Wang Y, Ling J, Hwang Y, Radermacher R, Takeuchi I and Cui J 2016 A review of elastocaloric cooling materials, cycles and system integrations *Int. J. Refrig.* **64** 1–19
- [59] Schmidt M, Kirsch S-M, Seelecke S and Schütze A 2016 Elastocaloric cooling: from fundamental thermodynamics to solid state air conditioning *Sci. Technol. Built Environ.* **22** 475–88
- [60] Ossmer H, Wendler F, Gueltig M, Lambrecht F, Miyazaki S and Kohl M 2016 Energy-efficient miniature-scale heat pumping based on shape memory alloys *Smart Mater. Struct.* **25** 085037
- [61] Lu B and Liu J 2017 Elastocaloric effect and superelastic stability in Ni-Mn-In-Co polycrystalline Heusler alloys: hysteresis and strain-rate effects *Sci. Rep.* **7** 2084
- [62] Tušek J, Engelbrecht K, Millán-Solsona R, Mañosa L, Vives E, Mikkelsen L P and Pryds N 2015 The elastocaloric effect: a way to cool efficiently *Adv. Energy Mater.* **5** 1500361
- [63] Miyazaki S, Otsuka K and Suzuki Y 1981 Transformation pseudoelasticity and deformation behavior in a Ti-50.6at%Ni alloy *Scr. Metall.* **15** 287–92
- [64] Zhou M, Li Y S, Zhang C and Li L F 2018 Elastocaloric effect and mechanical behavior for NiTi shape memory alloys *Chin. Phys. B* **27** 106501
- [65] Brinson L C, Schmidt I and Lammering R 2004 Stress-induced transformation behavior of a polycrystalline NiTi shape memory alloy: micro and macromechanical investigations via *in situ* optical microscopy *J. Mech. Phys. Solids* **52** 1549–71
- [66] Qian S, Yuan L, Hou H and Takeuchi I 2018 Accurate prediction of work and coefficient of performance of elastocaloric materials with phase transformation kinetics *Sci. Technol. Built Environ.* **24** 673–84
- [67] Suzuki T and Masumoto K 1972 Composition dependence of density in NiTi and CoTi *Metall. Mater. Trans. B* **3** 2009–10
- [68] Terada Y, Ohkubo K, Nakagawa K, Mohri T and Suzuki T 1995 Thermal conductivity of B2-type aluminides and titanides *Intermetallics* **3** 347–55
- [69] Berman H A, West E D and Rozner A G 1967 Anomalous heat capacity of TiNi *J. Appl. Phys.* **38** 4473–6
- [70] Smith J F, Lück R, Jiang Q and Predel B 1993 The heat capacity of solid Ni-Ti alloys in the temperature range 120–800 K *J. Phase Equilib.* **14** 494–500
- [71] Faulkner M G, Amalraj J J and Bhattacharyya A 2000 Experimental determination of thermal and electrical properties of Ni-Ti shape memory wires *Smart Mater. Struct.* **9** 632–9
- [72] Hou H et al 2019 Fatigue-resistant high-performance elastocaloric materials made by additive manufacturing *Science* **366** 1116–21
- [73] Qian S et al 2016 Elastocaloric effect in CuAlZn and CuAlMn shape memory alloys under compression *Phil. Trans. R. Soc. A* **374** 20150309
- [74] Frenzel J, Eggeler G, Quandt E, Seelecke S and Kohl M 2018 High-performance elastocaloric materials for the engineering of bulk- and micro-cooling devices *MRS Bull.* **43** 280–4
- [75] Chluba C, Ge W, Lima de Miranda R, Strobel J, Kienle L, Quandt E and Wuttig M 2015 Ultralow-fatigue shape memory alloy films *Science* **348** 1004–7
- [76] Mahtabi M J, Shamsaei N and Mitchell M R 2015 Fatigue of nitinol: the state-of-the-art and ongoing challenges *J. Mech. Behav. Biomed. Mater.* **50** 228–54
- [77] Robertson S W, Pelton A R and Ritchie R O 2012 Mechanical fatigue and fracture of nitinol *Int. Mater. Rev.* **57** 1–37